

Thecal plate morphology, molecular phylogeny, and toxin analyses reveal two novel species of *Alexandrium* (Dinophyceae) and their potential for toxin production

メタデータ	言語: English 出版者: 公開日: 2024-04-15 キーワード (Ja): キーワード (En): 作成者: Abdullah, Nursyahida, Tung Teng, Sing, Hamilton Hanifah, Afiqah, Kuo Law, Ing, Hii Tan, Toh, Krock, Bernd, M. Harris, Thomas, 長井, 敏, Teen Lim, Po, Tillmann, Urban, Pin Leaw, Chui メールアドレス: 所属: Universiti Malaysia Sarawak, Universiti Malaysia Sarawak, Universiti Malaysia Sarawak, University of Malaya, Universiti Putra Malaysia, Helmholtz Centre for Polar and Marine Research, Vanderbilt University, 水産研究・教育機構, University of Malaya, Helmholtz Centre for Polar and Marine Research, University of Malaya
URL	https://fra.repo.nii.ac.jp/records/2002145

Harmful Algae

Thecal plate morphology, molecular phylogeny, and toxin analyses reveal two novel species of *Alexandrium* (Dinophyceae) and their potential for toxin production

--Manuscript Draft--

Manuscript Number:	HARALG-D-23-00084R1
Article Type:	Research Paper
Keywords:	<i>Alexandrium</i> ; goniodomins; Harmful Algal Bloom; ITS secondary structure; paralytic shellfish toxins; Taxonomy; thecal plates
Corresponding Author:	Chui Pin Leaw, Ph.D. Bachok, Kelantan MALAYSIA
First Author:	Nursyahida Abdullah, MSc
Order of Authors:	Nursyahida Abdullah, MSc Sing Tung Teng, Ph.D. Afiqah Hamilton Hanifah, MSc Ing Kuo Law, MSc Toh Hii Tan, Ph.D. Bernd Krock, Ph.D. Thomas M. Harris, Ph.D. Satoshi Nagai, Ph.D. Po Teen Lim, Ph.D. Urban Tillmann, Ph.D. Chui Pin Leaw, Ph.D.
Abstract:	<p>This study describes two novel species of marine dinophytes in the genus <i>Alexandrium</i>. Morphological characteristics and phylogenetic analyses support the placement of the new taxa, herein designated as <i>Alexandrium limii</i> sp. nov. and <i>A. ogatae</i> sp. nov. <i>Alexandriumlimii</i>, a species closely related to <i>A. taylorii</i>, is distinguished by having a shorter 2'/4' suture length, narrower plates 1' and 6', with larger length: width ratios, and by the position of the ventral pore (Vp). While <i>A. ogatae</i> is distinguishable with its metasert plate 1' having almost parallel lateral margins, and by lacking a Vp. Production of paralytic shellfish toxins (PSTs), cycloimines, and goniodomins (GDs) in clonal cultures of <i>A. ogatae</i>, <i>A. limii</i>, and <i>A. taylorii</i> were examined analytically and the results showed that all strains contained GDs, with GDA as major variants (6–14 pg cell⁻¹) for all strains except the Japanese strain of <i>A. limii</i>, which exclusively had a desmethyl variant of GDA (1.4–7.3 pg cell⁻¹). None of the strains contained detectable levels of PSTs and cycloimines.</p>



Dr. Christopher J. Gobler
Editor
Harmful Algae

22 June 2023

SUBMISSION OF A REVISED MANUSCRIPT HARALG-D-23-00084

Dear Dr. Gobler,

I am pleased to submit the revised manuscript, with the title "**Thecal plate morphology, molecular phylogeny, and toxin analyses reveal two novel species of *Alexandrium* (Dinophyceae) and their potential for toxin production**", to be considered for publication in Harmful Algae as an original research paper.

In this revision, we have addressed the comments by the reviewers and revised the manuscript accordingly. The point-to-point responses to the reviewer's comments are listed in a separate document, together with the revised manuscript have now been uploaded to the system.

Your kind consideration is highly appreciated.

Yours sincerely,

Chui Pin Leaw, Ph.D.
Bachok Marine Research Station,
Institute of Ocean and Earth Sciences,
University of Malaya,
16310 Bachok, Kelantan, Malaysia.

Email: cpleaw@um.edu.my, chuiplinleaw@gmail.com

RESPONSES TO REVIEWERS' COMMENTS

Manuscript ID: HARALG-D-23-00084

Manuscript Title: Thecal plate morphology, molecular phylogeny, and toxin analyses reveal two novel species of *Alexandrium* (Dinophyceae) and their potential for toxin production

Reviewer #2:

The manuscript includes the description of two new species of *Alexandrium*, *A. limii* and *A. ogatae*, based on both morphological (light microscopy and SEM; detailed morphometry) and molecular data. The authors also examined (morphology and molecular phylogeny) additional strains of two closely related species, *A. taylorii* and *A. pseudogonyaulax* highlighting morphological characters that can be used to differentiate the species. The authors also tested the presence of different toxins (PSTs, gymnodimines, spirolides, and goniodomins in *A. limii*, *A. ogatae*, and *A. taylorii*, showing that the three species produce only goniodomins. The manuscript includes a discussion on the species included in the subgenus *Gessnerium* (sensu Balech 1985) showing that molecular phylogenies do not support this subgenus and that there is a need for further molecular studies (and toxin characterization) to properly define the phylogenetic position of several species.

The manuscript is clearly written, and the authors provide excellent pictures in epifluorescence microscopy and SEM to illustrate plate patterns of the various species. Additional information is provided as supplementary materials. Results are important for our appreciation of the diversity of *Alexandrium* species.

Response: We are grateful for your encouraging report and delighted to hear that you think our work is valuable. We now revised the manuscript based on your comments below. Thank you for the time and effort you expended on our behalf.

I have some minor comments that the authors should address when presenting a revised version of the manuscript.

Line 39: delete 'While'

Response: revised accordingly.

Line 58: Moestrup et al 2009 is not reported in the reference list. I suggest referring to the IOC-UNESCO Reference list for harmful microalgae: Fraga, S. (Ed) (2023). *Alexandrium & Pyrodinium*, in IOC-UNESCO Taxonomic Reference List of Harmful Micro Algae. Available online at <https://www.marinespecies.org/hab>. Accessed on XXXX

Response: The reference has now been included and cited as suggested.

Several references are not included in the Reference list: please check and add them (e.g., Line 70: Yñiguez et al., 2021; Line 72: Trainer and Yoshida, 2014; Sanseverino et al., 2016 ...)

Response: Thank you for pointing out the missing citations. The references are now added to the Reference list.

Line 361, 'additional specimens examined': it is not clear to me what Shioya Bay (Japan) refers to. I suggest listing here the other strains of *A. limii* reported in Table 1. In the phylogenetic tree, three strains of Atay99Shio-0x are included; they should be listed in Table 1. Specify that Atay99Shio-01 and Atay99Shio-03 were only used for molecular analyses: correct?

Response:

The information is now included in the text (line 361) and Table 1 is revised as suggested.

Line 370: list the strains used for morphological/morphometric examination.

Response:

The strain information is now added in the text (lines 365-366, 379).

In the illustration of *A. ogatae* morphology, specify that morphometric data refer to strains LASpbB10 and LASpbB5: correct? Check the strain names reported on Fig. 11A; LASpbB10 is reported as LABpbB10. List also for *A. ogatae* the additional strains examined and specify the ones that were only used for molecular analyses.

Response:

The information is now added in the text (lines 462-464).

Strain names in Fig. 11A have been revised.

Line 443: close the parenthesis after the date.

Response: Added accordingly.

Line 470: I suggest eliminating the word 'observed', i.e., 'There was no Vp in the specimens examined'

Response: Deleted accordingly.

Line 479: should be Fig. 11A

Response: Revised accordingly.

Line 509: specify that morphometric analyses were done on both the strains listed in Table 1.

Response:

The strain information is now added (line 522).

Reviewer #3:

Two new *Alexandrium* species, *A. limii* and *A. ogatae*, are described from Malaysia with their thecal morphology, phylogeny and production of gonyodomins. Molecular phylogeny showed the difference of *A. limii* from *A. taylori*, and *A. ogatae* from other *Alexandrium* in the Gessnerium, although no molecular data from *A. foedum*. SEM photos clearly showed their fine thecal structure, and the manuscript was carefully prepared with citation of related taxonomic works in *Alexandrium*. This work provides taxonomic information of the toxigenic genus, which will contribute to assess their ecology and distribution in future.

Response: Thank you for the positive comments. We are glad that you think our work is worthwhile for future ecological and distribution studies. We acknowledged your concerns, and we have now revised and responded to your comments as below.

Since the ventral pore position is an important character separating *A. limii* from *A. taylori*, careful comparison is required. Explain how many *A. limii* cells had the ventral pore contacting also with the 1', and there were no *A. taylorii* cells having the ventral pore between the 2' and 4'?

Response: Thank you for this constructive comment. We now included more descriptions of the character – Vp position of *A. limii* and *A. taylorii*, with detailed observations and comparison [see lines 392-296, 399-401, 557-564] and the discussion [lines 666-678].

The Vp of *A. limii* is usually located almost midway between 1' and Po when the 2'/4' suture is longer. Although in some observations (about 40% of cells observed), it could be very close to the posterior tip of plate 1' when the 2'/4' suture is very short. But this is never the case for *A. taylorii*. Only 2-4% of *A. taylorii* cells examined the Vp was located on the suture between plates 2' and 4'. We now included the number of cells observed.

58, '(Moestrup et al., 2009)', currently '(Lundholm et al., 2009)'.

Response: Revised.

87, 'the pore plate (Po)', 'the apical pore plate (Po)'.

Response: Revised accordingly.

97, 'Balech', Balech (1995)?

Response: Revised accordingly.

114; add ',' after '*A. foedum*'.

Response: A comma is now added.

214-215, 'tree-bisection reconnection' to 'tree bisection and reconnection (TBR)'.

Response: Revised accordingly.

236, neighbor-joining (NJ) using general time reversible (GTR).

Response: Revised accordingly.

241, (Coleman, 2009; Keller et al., 2009)

Response: Revised accordingly.

256, ideally avoid the use of new name *A. limii* before the description.

Response: Thank you, the name is now removed.

367, (Figs 1A, 2E-H), to (Figs 1A, 2E, H), the round structure was not seen in Fig. 2F, G.

Response: Revised accordingly (line 370).

374, (Figs 2C, D, 4A)

Response: Revised accordingly (line 377).

388, Vp was not seen in Fig. 4B. Is it in Fig. 4C? 'in some cases', how many cells in all observations? This is an important character showing the difference from *A. taylorii*.

Response: The number of cell observations is now included in the text (lines 392-396).

426, (Figs 3F, G, 4G)

Response: Revised accordingly (line 436).

456, the nucleus is difficult to see in Fig. 6A, B.

Response: We now revised as (Fig. 6C) in the text (line 468).

535, Tillmann et al. (2020)

Response: The dot is now added.

543, 'A large Vp', no observed cells with the Vp on the suture between 2' and 4' plates?

Response: There was a very low percentage of *A. taylorii* cells (<4%) observed with the Vp on the suture between 2' and 4'. We now included the description (see lines 557-564) and discussion in the text (lines 666-678).

588-589, *A. limii* was a sister to *A. taylorii* in the SSU tree, and sister to *A. pseudogonyaulax* in the LSU tree (Figs 12, S1, S2), revise the sentences.

Response: Thank you for pointing out the mistake, it has been revised accordingly (lines 608, 609).

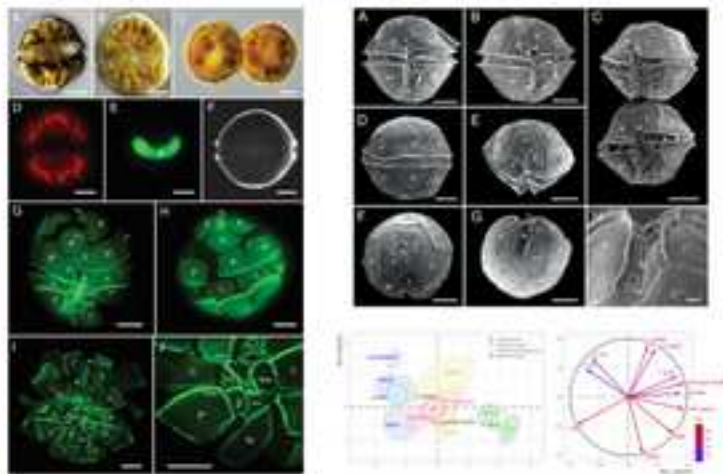
667, particularly

Response: Amended (line 692).

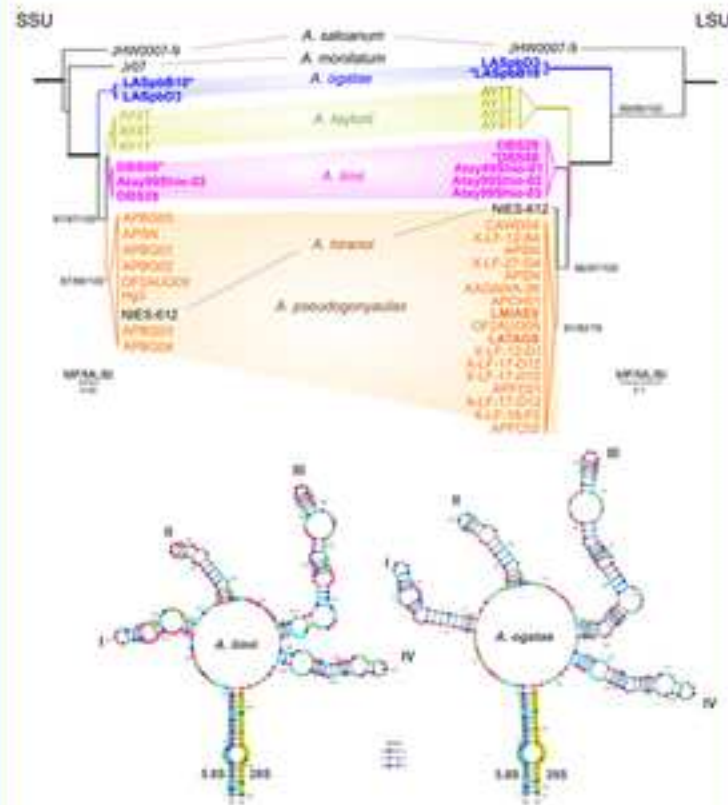
736, Tillmann et al.

Response: Amended.

Morphological characterization



Molecular phylogenetic inferences



Toxin analyses

GYMs
STXs
PnTXs



Thecal plate morphology, molecular phylogeny, and toxin analyses reveal two novel species of *Alexandrium* (Dinophyceae) and their potential for toxin production

Highlights

1. Two new *Alexandrium* species, *A. limii* and *A. ogatae*, were described.
2. Goniodomins (GDs) were detected in the strains of *A. limii*, *A. ogatae*, and *A. taylorii*, with GDA as the major variant, but PSTs and cycloimines were undetectable.
3. GD-producing *Alexandrium* species were reported, for the first time, in the Southeast Asian region.
4. GD production is likely a common trait for species of the molecularly-defined *Gessnerium* clade of *Alexandrium*.

1 RESEARCH ARTICLE

2

3 **Thecal plate morphology, molecular phylogeny, and toxin analyses reveal two novel species**
4 **of *Alexandrium* (Dinophyceae) and their potential for toxin production**

5

6 Nursyahida Abdullah ^a, Sing Tung Teng ^{a,*}, Afiqah Hamilton Hanifah ^a, Ing Kuo Law ^b, Toh Hii
7 Tan ^c, Bernd Krock ^d, Thomas M. Harris ^e, Satoshi Nagai ^f, Po Teen Lim ^b, Urban Tillmann ^d,
8 Chui Pin Leaw ^{b, *}

9

10 ^a *Faculty of Resource Science and Technology, Universiti Malaysia Sarawak, 94300 Kota*
11 *Samarahan, Sarawak, Malaysia*

12 ^b *Bachok Marine Research Station, Institute of Ocean and Earth Sciences, University of Malaya,*
13 *16310 Bachok, Kelantan, Malaysia*

14 ^c *Department of Animal Science and Fishery, Faculty of Agricultural Science and Forestry,*
15 *Universiti Putra Malaysia, 97008 Bintulu, Sarawak, Malaysia*

16 ^d *Section Ecological Chemistry, Alfred Wegener Institute, Helmholtz Centre for Polar and*
17 *Marine Research, 27570 Bremerhaven, Germany*

18 ^e *Department of Chemistry, Vanderbilt, University, Nashville, Tennessee 37235, United States;*
19 *Virginia Institute of Marine Science (VIMS), Gloucester Point, Virginia 23062, United States*

20 ^f *Japan Fisheries Research and Education Agency, 2-12-4 Fukuura, Kanazawa, Yokohama,*
21 *Kanagawa 236-8648, Japan*

22

23 *Authors for correspondence: tsteng@unimas.my; cpleaw@um.edu.my

24 **Highlights**

- 25 1. Two new *Alexandrium* species, *A. limii* and *A. ogatae*, were described.
- 26 2. Goniodomins (GDs) were detected in the strains of *A. limii*, *A. ogatae*, and *A. taylorii*,
- 27 with GDA as the major variant, but PSTs and cycloimines were undetectable.
- 28 3. GD-producing *Alexandrium* species were reported, for the first time, in the Southeast
- 29 Asian region.
- 30 4. GD production is likely a common trait for species of the molecularly-defined
- 31 *Gessnerium* clade of *Alexandrium*.

32

33 **Abstract**

34 This study describes two novel species of marine dinophytes in the genus *Alexandrium*.
35 Morphological characteristics and phylogenetic analyses support the placement of the new taxa,
36 herein designated as *Alexandrium limii* sp. nov. and *A. ogatae* sp. nov. *Alexandrium limii*, a
37 species closely related to *A. taylorii*, is distinguished by having a shorter 2'/4' suture length,
38 narrower plates 1' and 6'', with larger length: width ratios, and by the position of the ventral pore
39 (Vp). *Alexandrium ogatae* is distinguishable with its metasert plate 1' having almost parallel
40 lateral margins, and by lacking a Vp. Production of paralytic shellfish toxins (PSTs), cycloimines,
41 and goniodomins (GDs) in clonal cultures of *A. ogatae*, *A. limii*, and *A. taylorii* were examined
42 analytically and the results showed that all strains contained GDs, with GDA as major variants
43 (6–14 pg cell⁻¹) for all strains except the Japanese strain of *A. limii*, which exclusively had a
44 desmethyl variant of GDA (1.4–7.3 pg cell⁻¹). None of the strains contained detectable levels of
45 PSTs and cycloimines.

46

47 **Keywords:** *Alexandrium*; goniodomins; harmful algal bloom; ITS secondary structure; paralytic
48 shellfish toxins; Taxonomy; thecal plates

49

50 1. INTRODUCTION

51 The genus *Alexandrium* Halim is a marine dinophyte commonly found in coastal waters
52 around the world (Hallegraeff, 1993; Anderson et al., 2012). *Alexandrium* has been extensively
53 studied in recent decades for its ability to produce paralytic shellfish toxins (PSTs) in several
54 toxigenic species. PSTs are a group of potent neurotoxins also known as saxitoxin (STX)
55 variants. The toxin accumulates in shellfish vectors, transfers to humans, and causes severe
56 neurological symptoms, including paralysis and respiratory failure, causing paralytic shellfish
57 poisoning (PSP). [Of the 32 taxonomically accepted species to date \(Mertens et al., 2020\), 16 are](#)
58 [listed as harmful species \(Lundholm et al., 2023\), at least one-third are capable to produce PSP](#)
59 [toxins](#). In recent decades, there have been numerous PSP outbreaks worldwide, particularly in
60 Southeast Asia, resulting in human fatalities (e.g., Lim et al., 2007, 2012, 2020; Yñiguez et al.,
61 2021). Furthermore, blooms of several *Alexandrium* species are known to cause significant
62 losses to aquaculture industries in America, Europe, Asia ([Trainer and Yoshida, 2014; Trainer,](#)
63 [2020](#)), Australia, and New Zealand (MacKenzie et al., 2004; [Jin et al., 2008; Condie et al., 2019](#)).
64 To cite an instance, the 2016 bloom of *A. catenella* (Whedon & Kofoid) Balech in Chile was a
65 notable case that badly hit the salmon aquaculture industries. This bloom killed over 30,000 tons
66 of farmed salmon, causing losses of over \$800 million (Díaz et al., 2019). There are several
67 species of *Alexandrium* that produce harmful metabolites other than PSTs, such as cycloimines
68 (spiroptides, gymnodimines), goniodomins, and some poorly characterized lytic compounds,
69 which are believed to release into the marine environment and affect a wide range of marine
70 organisms including fishes (reviewed in Long et al., 2021).

71 Species delineation in *Alexandrium* traditionally relied on distinct features in the thecal
72 plate morphology. For example, the first and third apical plates (1', 3'), the sixth precingular

73 plate (6''), and the sulcal plates are among the plates used to delineate species of *Alexandrium*
74 (Balech, 1985, 1995). Some of these characters, however, have been regarded as labile and
75 taxonomically uninformative (e.g., Delgado et al., 1997; Hansen et al., 2003; Leaw et al., 2005;
76 Kremp et al., 2014; John et al., 2014). Integrative taxonomy based on multiple lines of evidence
77 encompassing morphology, molecular phylogenies, and mating compatibility has been
78 increasingly applied in dinophyte taxonomy. The molecular phylogenetic approach has become
79 one of the most widely accepted approaches to affirm the species validity of *Alexandrium*.
80 Among the numerous genetic markers, the nuclear-encoded ribosomal DNAs (SSU, ITS, and
81 LSU rDNA) have been widely used to infer the phylogenetic relationships of the species in
82 *Alexandrium* (Usup et al., 2002; Leaw et al., 2005; Lilly et al., 2007; Gu et al., 2013; John et al.,
83 2014; Kremp et al., 2014; Branco et al., 2020; Tillmann et al., 2021). Integrating both the
84 morphology and molecular characteristics of species in the genus has proven powerful in
85 delineating the species boundaries in some studies (Fraga et al., 2015; Litaker et al., 2018).

86 In *Alexandrium* taxonomy, species that share a metasert or exsert plate 1' (not
87 rhomboidal/insert) which is constantly disconnected from the apical pore plate (Po), were
88 classified in the subgenus *Gessnerium sensu* Balech (1995). Balech chose this subgenus name
89 based on the heterotypic junior synonym (*Gessnerium mochimaense* Halim) of the first described
90 species of this group (*Alexandrium monilatum* (J.F.Howel) Balech). The nine species assigned to
91 *Gessnerium* by Balech (1995) are *A. balechii* (Steidinger) Balech, *A. foedum* Balech, *A. hiranoi*
92 K.Kita & Y.Fukuyo, *A. insuetum* Balech, *A. margalefii* Balech, *A. monilatum*, *A.*
93 *pseudogonyaulax* (Biecheler) Horiguchi ex K.Yuki & Y.Fukuyo, *A. satoanum* K.Yuki &
94 Y.Fukuyo, and *A. taylorii* Balech. Other species described later with the *Gessnerium*-type 1'
95 include *A. camurascutulum* MacKenzie & K.Todd, *A. concavum* (Gaarder) Balech emend.

96 Nguyen Ngoc & Larsen, *A. globosum* Nguyen-Ngoc & J.Larsen, and *A. pohangense* A.S.Lim &
97 H.J.Jeong. The morphological concept of Balech (1995) in differentiating between the subgenera
98 *Alexandrium* and *Gessnerium* somehow failed to reflect two distinct genetically inferred
99 evolutionary units. Several species of the subgenus *Gessnerium sensu* Balech (*A. hiranoi*, *A.*
100 *monilatum*, *A. pseudogonyaulax*, *A. satoanum*, *A. taylorii*) formed a highly supported
101 monophyletic clade (a *Gessnerium* clade), but several species, for instance, *A. insuetum*, *A.*
102 *margalefii*, and *A. pohangense* were grouped with other species in the subgenus *Alexandrium*
103 *sensu* Balech in the rDNA phylogenetic trees (Kim et al., 2005; Leaw et al., 2005; Tillmann et al.,
104 2021). From a chemical perspective, species of the *Gessnerium* clade are known to produce
105 goniiodomin A (GDA), this includes *A. hiranoi*, *A. monilatum*, *A. pseudogonyaulax*, and *A.*
106 *taylorii* (e.g., Hsia et al., 2006; Espina et al., 2016; Triki et al., 2016; Krock et al., 2018;
107 Tillmann et al., 2020). Although little is known about their toxicity potentials and impacts on
108 ecology and socio-economy (Tillmann et al., 2020), it was shown that GDs can cause liver and
109 thymus damage in mice (Terao et al., 1989), are cytotoxic (Espiña et al., 2016), and have been
110 associated with mortality in aquatic invertebrates (Harding et al., 2009), with significant impacts
111 on local ecosystems.

112 For identification of the full species diversity within this *Gessnerium* clade, there is a
113 need to re-examine and integrate molecular information of the other described species with a
114 *Gessnerium*-type 1' plate (e.g., *A. balechii*, *A. camurascutulum*, *A. concavum*, *A. foedum*, *A.*
115 *globosum*). Moreover, large differences in the GenBank sequence entries annotated as *A. taylorii*
116 indicate the possibility of multiple distinct lineages (Tillmann et al., 2020). A morphospecies that
117 resembled *A. taylorii* was reported by Lim et al. (2004) from Malaysian Borneo; the strains were
118 previously designated as *A. taylorii* based on the thecal morphology that resembled the species

119 (Balech, 1995). But no molecular data from the strains were available at that time for
120 phylogenetic inference. In the present study, the site where the strains were isolated was revisited,
121 and new strains were established in culture. Together, several *Alexandrium* strains from different
122 geographical regions were also established and examined for species identification. Integrating
123 the morphological and molecular evidence in this study revealed two novel species of
124 *Alexandrium*. Further, the presence of relevant toxins for different strains of both new species
125 was determined.

126

127 **2. MATERIALS AND METHODS**

128 **2.1. Algal cultures**

129 Plankton samples were collected by 20- μ m mesh plankton net hauls. Live samples were
130 brought back to the laboratory for culture establishment. Single *Alexandrium*-like cells were
131 isolated using a finely drawn Pasteur pipette under an Olympus IX51 inverted light microscope
132 (Olympus, Tokyo, Japan) and transferred to a 96-well tissue culture plate containing GPM
133 medium (Loeblich, 1975).

134 Malaysian strains were grown in a sterile natural seawater base (salinity of 30) enriched
135 with L1 medium, while strains AY1T, AY7T, and Atay99Shio-02 were grown using a K-based
136 medium (Keller et al., 1987) prepared from 0.2 μ m sterile-filtered North Sea water (salinity of
137 33). The original K-medium receipt was slightly modified by replacing the organic phosphorous
138 source (β -Glycerophosphate) with 3.62 μ M di-sodium hydrogen phosphate (Na_2HPO_4). Strains
139 were grown at 20 °C (AY1T, AY7T), 25 °C (Atay99Shio-02), or 26 °C (Malaysian strains)
140 under moderate photon flux densities (80 μ mol photons $\text{m}^{-2} \text{s}^{-1}$) at a 16:8 h (temperate strains) or

141 12:12 h (tropical strains) light:dark cycle in a controlled environment growth chamber (MIR 252,
142 Sanyo Biomedical, Wood Dale, USA or SRI21D-2 Shel Lab, Sheldon Manufacturing, CA, USA).

143 All *Alexandrium* strains used in this study, with their strain codes and locality, are listed
144 in Table 1.

145

146 **2.2. Morphological observation**

147 **2.2.1. Light microscopy (LM)**

148 Live cells (7–10 days cultures) were examined under an IX51 inverted microscope
149 (Olympus, Tokyo, Japan) or Axiovert 2 microscope (Zeiss, Göttingen, Germany) equipped with
150 epifluorescence and differential interference contrast optics. Images of cells were captured by an
151 INFINITY-3 digital camera (Teledyne Lumenera, Ottawa, Canada) or Axiocam MRc5 (Zeiss)
152 digital camera to record cell shape, and nuclei position and shape.

153 To determine the shape and position of the nucleus, the culture samples were stained with
154 0.1% SYBR Safe DNA stain (Invitrogen, MA, USA) in the dark and observed immediately using
155 the same microscope equipped with 450–490 nm excitation and 510–550 nm emission. To
156 observe thecal plate arrangement, cells were stained with Solophenyl Flavine 7GFE (Direct
157 Yellow 96, Sigma-Aldrich, MO, USA), then examined under the microscope with 450–490 nm
158 excitation and 510–550 nm emission.

159

160 **2.2.2. Scanning electron microscopy (SEM)**

161 Cells were preserved in acidic Lugol's solution with a final concentration of 1%. The
162 preserved cells were filtered on a 3 µm-pore size polycarbonate membrane (Whatman, USA) and
163 washed with distilled water twice for 20 min each. The samples were then dehydrated in a

164 graded ethanol series (30%, 50%, 75%, 90%, 95%, 99%, 99.5%, 15 min at each step; followed
165 by $2 \times 99.5\%$, $2 \times 100\%$, 30 min). The samples were dried using a K580 Critical Point Dryer
166 (Quorum Technologies Ltd., UK). The membrane was mounted on a stub and coated with
167 platinum-palladium using a JEC-3000FC Auto Fine Coater (JEOL, Tokyo, Japan). Cells were
168 examined using a JSM-IT500HR Scanning Electron Microscope (JEOL, Tokyo, Japan).

169

170 **2.2.3. Morphometric data analysis**

171 Morphometric measurements of cell dimension and thecal plates were performed on
172 individual cells of nine strains of *Alexandrium* based on the light and SEM micrographs (Table
173 1). To explore if thecal morphometrics of *Alexandrium* species in this study exhibit differences
174 among strains and species, and to visualize patterns of variations, the dataset was analyzed by
175 using principal component analysis (PCA) as implemented in FactoMineR in R (Lê et al., 2008).
176 The dataset contained 512 cells and 11 morphological variables: cell length (L), cell width (W),
177 L:W, 1' length, 1' width, 1' L:W, 6'' length, 6'' width, 6'' L:W, length of suture adjoined 2' and 4'
178 (herein referred 2'/4' suture), and the ratio of 2'/4' suture to 1' length (Suppl. Material 1).

179

180 **2.3. Molecular characterization**

181 **2.3.1. Genomic DNA isolation, gene amplification, and sequencing**

182 Genomic DNA was isolated from the exponential-phased cultures (7–10 days cultures).
183 Cells were harvested by centrifugation ($2,800 \times g$, 20 min) and DNA was isolated using the
184 Dneasy® Plant Mini Kit (Qiagen, Hilden, Germany) following the manufacturer's protocol. The
185 purified DNA was kept at $-20\text{ }^{\circ}\text{C}$ until further analysis.

186 The small subunit (SSU) ribosomal RNA gene (rDNA) was amplified using two primer
187 pairs: 18SAlexF1 (5' GCTTGTCTCAAAGATTAAGCCATGC 3') and 18SAlexR1 (5'
188 CATCCTTGGCAAATGCTTTCGCA 3'); 18SAlexF2 (5' GTCAGAGGTGAAATTCTTGGATT
189 3') and 18SAlexR2 (5' CCTTGTTACGACTTCTCCTTCCTC 3'). The large subunit (LSU) rDNA
190 in the domain D1–D3 was amplified using the primer pair, D1R and D3Ca (Scholin et al., 1994).
191 The internal transcribed spacers (ITS) region was amplified using the primer pair, AlexITSf1 (5'
192 GAGGAAGGAGAAGTCGTAACAAGG 3') and AlexITSr1 (5'
193 CATTCCAATGCCRAGGARTG 3'). The amplifications were carried out in a 25 μ L reaction
194 mixture containing 1 \times PCR buffer (Promega, Madison, WI, USA), 1.5 mM MgCl₂ (Promega),
195 0.2 mM of dNTPs (Fermentas, Thermo Fisher Scientific, MA, USA), 0.5 μ M of each primer, 1 U
196 *Taq* DNA polymerase (Promega), and 10–100 ng μ L⁻¹ DNA.

197 The amplification was performed using an Eppendorf Mastercycler® gradient
198 thermocycler (Eppendorf, Hamburg, Germany), with the amplification condition as follows:
199 Initial denaturation for 4 min at 94 °C, followed by 35 cycles of 35 s denaturation at 94 °C,
200 annealing at 55.5 °C for 30 s (18SAlexF1–18SAlexR1)/ 52.5 °C for 30 s (18SAlexF2–
201 18SAlexR2)/ 55 °C for 50 s (D1R–D3Ca)/ 55 °C for 45 s (AlexITSf1–AlexITSr1), extension at
202 72 °C for 35 s (18SAlexF–18SAlexR, D1R–D3Ca)/ 1.5 min (AlexITSf1–AlexITSr1), and a final
203 extension of 7 min at 72 °C.

204 Amplicons were purified with the Promega Wizard® PCR Preps DNA Purification
205 System prior to sequencing. DNA sequencing was performed by Sanger sequencing on both
206 strands using an ABI 3730XL DNA Analyzer (PE Biosystems, Vernon Hills, IL, USA).

207

208 **2.3.2. Sequence analysis and phylogenetic reconstructions**

209 Newly obtained sequences of the SSU, LSU, and ITS rDNA and related sequences
210 retrieved from the NCBI GenBank nucleotide database (Table 1, Table S1) were multiple-
211 aligned using Multiple Sequence Comparison by Log-Expectation, MUSCLE (Edgar, 2004).

212 Phylogenetic analyses of maximum parsimony (MP) and maximum likelihood (ML) were
213 performed using PAUP* ver. 4.0b.10 (Swofford, 2001). MP was performed using heuristic
214 searches with 1000 random-addition replications and branch-swapping with [tree bisection and](#)
215 [reconnection \(TBR\)](#). Bootstrap analysis was performed with 1,000 bootstrap replicates and 100
216 random additions of sequences run per bootstrap replicates. ML was performed using the best-fit
217 model calculated by the Akaike information criterion in jModelTest 2.1.3 (Darriba and Posada,
218 2014), with 1,000 random addition replications; heuristic searches were carried out with branch-
219 swapping and TBR. Bayesian analysis (BI) was performed using MrBayes 3.2.2 (Ronquist et al.
220 2012), based on the same best-fit model, a four-chain run for 10^7 generations was used and trees
221 were sampled every 100 generations; posterior probabilities (PP) were estimated with 20,000
222 generations burn-in.

223 All the SSU, LSU, and ITS rDNA datasets were used to calculate the sequence
224 divergences of closely related species based on uncorrected pairwise p-distances using MEGA11
225 (Tamura et al. 2021).

226

227 ***2.3.3. ITS2 transcript modelling and CBC analysis***

228 The nucleotide sequences of the ITS1-5.8S-ITS2 region obtained in this study and those
229 retrieved from the GenBank (Table 1, Table S1) were used to identify the ITS2 region by
230 annotating the 5.8S–LSU rRNA interaction (Keller et al., 2009). The ITS2 sequences were then

231 used to model the secondary structures of ITS2 RNA transcript by homology modeling using the
232 ITS2 Database V web interface (Ankenbrand et al., 2015) as outlined in Teng et al. (2016).

233 Orthologous alignment was guided by secondary structures of the ITS2 RNA transcripts
234 using 4SALE v1.5 sequences-structure alignment (Seibel et al., 2008). A sequences-structure
235 informative phylogenetic tree of ITS2 RNA transcript was reconstructed using ProfDistS v0.9.9
236 (Qt version) (Wolf et al., 2008) by [neighbor-joining \(NJ\)](#) using [general time reversible \(GTR\)](#)
237 evolutionary model, followed by 1,000 bootstrap replications. ML analysis was performed using
238 Phargorn (Schliep, 2011) in R, with nonparametric bootstrap analysis (100 bootstrap replications
239 and NNI optimization).

240 The ITS2 universal motifs of *Alexandrium* ITS2 transcripts were annotated based on
241 previous studies ([Coleman, 2009](#); [Keller et al., 2009](#)). The structures were illustrated using
242 VARNA (Darty et al., 2009). Compensatory base changes (CBCs) and hemi-CBCs (HCBCs)
243 were identified and mapped on the core ITS2 transcript (Teng et al., 2014). A CBC matrix table
244 based on pairwise comparison was constructed by 4SALE.

245

246 **2.4. Toxin analysis**

247 ***2.4.1. Toxin extraction***

248 For toxin analyses, strains were grown in 250 mL plastic culture flasks with the culture
249 conditions described above. Cell densities from cultures in the early stationary phase (ranging
250 from approximately 1×10^3 to 6×10^3 cells mL⁻¹) were determined by settling Lugol's iodine-
251 fixed samples and counting >400 cells under an inverted microscope. Cells were harvested by
252 centrifugation of multiple 50 mL subsamples (Eppendorf 5810R, 3,220 ×g, 10 min). The
253 different cell pellets of one strain were resuspended, and combined in one microtube, centrifuged

254 again (Eppendorf 5415, 16,000 $\times g$, 5 min), and stored frozen (-20 °C) until use. For all strains,
255 one cell pellet each was collected for analyses of lipophilic toxins and for PSP toxins (PSTs).
256 Lipophilic toxins of strain Atay99Shio-02 were determined for three different cell pellets
257 obtained from three independently grown cultures. The total number of cells harvested for these
258 strains and the corresponding detection limits of toxins are listed in Tables S2 and S3. Note that
259 the toxin profile of *A. pseudogonyaulax* strains could not be determined because both strains died
260 off in the course of this study.

261 Cell pellets were extracted with 300 μ L 0.03 M acetic acid for PST extraction and with
262 300 μ L methanol for the extraction of lipophilic toxins and lyzing Matrix D (Thermo Savant) in
263 a homogenizer (MagnaLyzer, Roche Diagnostics, Mannheim, Germany) for 45 s at 5,500 $m s^{-1}$.
264 The homogenates were centrifuged for 5 min at 13,200 $\times g$. The supernatants were transferred to
265 spin filters (0.45 μ m, UltraFree, Millipore, Eschborn, Germany) and centrifuged for 30 s at 5,700
266 $\times g$. The filtrates were transferred to HPLC vials and stored at -20 °C until analysis.

267

268 **2.4.2. Analysis of paralytic shellfish toxins**

269 PST analysis was performed by two independent methodological approaches: ion-pair
270 chromatography coupled to post-column derivatization and fluorescence detection (PCOX) and
271 hydrophilic interaction liquid chromatography coupled to tandem mass spectrometry (HILIC-
272 MS/MS).

273 The PCOX analysis was performed on a liquid chromatography system (LC1100
274 consisting of a G1379A degasser, a G1311A quaternary pump, a G1229A autosampler, and a
275 G1321A fluorescence detector, Agilent Technologies, Waldbronn, Germany), equipped with a
276 Phenomenex Luna C18 reversed-phase column (250 mm \times 4.6 mm id, 5 μ m pore size)

277 (Phenomenex, Aschaffenburg, Germany) with a Phenomenex SecuriGuard precolumn. The
278 column was coupled to a PCX 2500 post-column derivatization system (Pickering Laboratories,
279 Mountain View, CA, USA). Eluent A contained 6 mM octane-sulfonic acid, 6 mM heptane-
280 sulfonic acid, 40 mM ammonium phosphate, adjusted to pH 6.95 with dilute phosphoric acid,
281 and 0.75% tetrahydrofuran. Eluent B contained 13 mM octane-sulfonic acid, 50 mM phosphoric
282 acid, adjusted to pH 6.9 with ammonium hydroxide, 15% acetonitrile, and 1.5% tetrahydrofuran.
283 The flow rate was 1 mL min⁻¹ with the following gradient: 0–5 min isocratic A, 15–16 min
284 switch to B, 16–35 min isocratic B, 35–36 min switch to A, 36–45 min isocratic A. The injection
285 volume was 20 µL and the autosampler was cooled to 4 °C. The eluate from the column was
286 oxidized with 10 mM periodic acid in 555 mM ammonium hydroxide before entering the 50 °C
287 reaction coil, after which it was acidified with 0.75 M nitric acid. Both the oxidizing and
288 acidifying reagents entered the system at a rate of 0.4 mL min⁻¹. The toxins were detected by
289 dual-monochromator fluorescence (lex 333 nm; lem 395 nm). The data were processed with
290 Chemstation software (Agilent, Santa Clara, CA, USA) and calibrated against external standards.

291 The HILIC-MS/MS was performed on an Acquity UPLC Glycan BEH Amide column
292 (130 Å, 150 mm × 2.1 mm, 1.7 µm, Waters, Eschborn, Germany) equipped with an in-line 0.2
293 µm Acquity filter and thermostated at 60 °C with an isocratic elution to 5 min with 98% eluent B
294 followed by a linear gradient of 2.5 min to 50% B and 1.5 min isocratic elution. The flow rate
295 was 0.4 mL min⁻¹, and the injection volume was 2 µL. Mobile phase A consisted of water with
296 0.15% formic acid and 0.6% ammonia (25%). Mobile phase B consisted of water/acetonitrile
297 (3:7, v/v) with 0.1% formic acid. Mass spectrometric experiments were performed in the selected
298 reaction monitoring (SRM) mode on a Xevo TQ-XS triple quadrupole mass spectrometer
299 equipped with a Z-Spray source (Waters, Halesworth, MD, USA). Instrument parameters are

300 given in Table S4 and used mass transitions in Table S5. PSTs were quantified by external
301 calibration with standard mix solutions of 4 concentration levels consisting of the following
302 PSTs: STX, NEO, GTX2/3, GTX1/4, dcSTX, dcGTX2/3, B1, and C1/2. All individual standard
303 solutions were purchased from the Certified Reference Materials Program (CRMP) of the
304 Institute for Marine Biosciences, National Research Council (Halifax, Canada).

305

306 *2.4.3. Analysis of lipophilic toxins*

307 LC-MS/MS analysis for cycloimines was performed on a reversed-phase C18 column
308 (Purospher STAR RP-18 end-capped (2 μm) Hibar HR 50-2.1, Merck, Darmstadt, Germany)
309 equipped with a guard column (EXP Pre-column Filter Cartridge, Merck) and thermostated at
310 40 °C with an isocratic elution to 5 min with 5% eluent B followed by a linear gradient of 2.0
311 min to 100% B and 3.0 min isocratic elution prior to returning to initial conditions. The flow rate
312 was 0.6 mL min⁻¹, and the injection volume was 0.5 μL . Mobile phase A consisted of 500 mL
313 water with 955 μL formic acid and 75 μL 25% ammonia. Mobile phase B consisted of 475 mL
314 acetonitrile, 25 mL deionized water, 955 μL formic acid and 75 μL 25% ammonia. Mass
315 spectrometric experiments were performed in the selected reaction monitoring (SRM) mode in
316 positive polarity on a Xevo TQ-XS triple quadrupole mass spectrometer equipped with a Z-
317 Spray source (Waters). Instrument parameters are given in Table S6 and used mass transitions in
318 Table S7. A standard solution of 100 pg μL^{-1} SPX 1 and 50 pg μL^{-1} GYM A (CRMP, IMB-
319 NRC, Halifax, NS, Canada) were used for the determination of detection limits.

320 For the analysis of GDs, an alkaline elution system was used with eluent A consisting of
321 aqueous 6.7 mM ammonia and eluent B of 6.7 mM ammonia in ACN/water (9/1 v/v). The flow
322 rate was 0.6 mL min⁻¹ and initial conditions of 20% B were held for 1.5 min. Then a linear

323 gradient from 20% B to 90% B was performed within 2 min (until 3.5 min) followed by isocratic
324 elution with 90% B for 0.5 min (until 4 min) prior to returning to initial conditions within 0.1
325 min and 0.9 min equilibration time (total run time: 5 min). The mass spectrometric parameters
326 are given in Table S8, and the applied transitions are in Table S9. The collision energies for
327 ammonium adducts were 30 eV and for sodium adducts 45 eV. Data were acquired and analyzed
328 with MassLynx v.4.2 (Waters).

329

330 **3. Results**

331 **3.1. Morphological characterization of *Alexandrium* species**

332 Four morphotypes of *Alexandrium* were revealed from ten strains examined in this study
333 (Table 1). Two morphotypes were identified as *A. pseudogonyaulax* and *A. taylorii* (two strains
334 each) while two other morphotypes are proposed here to represent new species, *A. limii* sp. nov.
335 and *A. ogatae* sp. nov., and the morphological descriptions of all species examined are presented
336 below.

337

338 *Alexandrium limii* sp. nov.

339 S.T.Teng, Tillmann, N.Abdullah, S.Nagai et Leaw

340 (Figs 1–5)

341 DESCRIPTION: Phototrophic, thecate dinophyte. Cells solitary or in short two-cell chains after
342 division, spherical to subspherical in outline, 21–45 μm long, 21–46 μm wide. Thin theca with
343 smooth surface and minute pores. Cingulum median, descending one cingular width, with
344 cingular lists along anterior and posterior sutures. Thecal tabulation: Po, 4', 6'', 6C, 8–10S, 5''',
345 2'''''. Plate 1' pentagonal, without contact with apical pore plate, left anterior margin shorter than

346 right. Plate 6'' longer than wide. Ventral pore usually located median on suture of 2' and 4'. Left
347 anterior lateral sulcal plate (Ssa) large. Anterior sulcal plate (Sa) incised right posterior end of 1'.
348 Sulcal lists present on right margin of plates 1''', 1''''', and left margin of 5'''. Posterior sulcal plate
349 (Sp) elongated, oblique to right.

350

351 HOLOTYPE: Glutaraldehyde-fixed material of strain DBS08 (labeled 'holotype of *Alexandrium*
352 *limii*, prepared from strain DBS08, Batang Salak, Sarawak, 15/3/2017') deposited at the Aquatic
353 Botany Culture Collection, University Malaysia Sarawak, Malaysia.

354

355 TYPE LOCALITY: Batang Salak (1° 36' 31.4886" N, 110° 19' 36.6774" E), Sarawak, Malaysia
356 Borneo.

357

358 ETYMOLOGY: The species is named in honor of Dr. Po Teen Lim (Malaysia) for his contribution
359 to the HABs research, development, and capacity building in Malaysia.

360

361 ADDITIONAL SPECIMENS EXAMINED: [strain Atay99Shio-02](#) from Shioya Bay (Japan) ([Table 1](#),
362 [Figs 2–3](#)).

363

364 ***Alexandrium limii* morphology**

365 [Light and epi-fluorescence micrographs of strain DBS08 are presented in Fig. 1, and](#)
366 [strain Atay99Shio-02 in Figs 2 and 3.](#) Cells were spherical to subspherical in outline (Figs 1–2),
367 solitary, or in two-cell chains (Figs 1C, 2D–E). Cells were brownish orange in colour (Fig. 1A–
368 C), with numerous granular and ellipsoidal chloroplasts radially distributed from the center (Figs

369 1D, 2A). A round structure (potentially a pyrenoid) was located centrally or in the hyposome
370 (Figs 1A, 2E, H). The nucleus was located in the cingular plane (Figs 1A–B, 2A–B), with both
371 ends visible in the ventral view under LM (Fig. 1A); when stained with SYBR, the nucleus
372 appears in a hemi-toroidal shape in the apical view (Fig. 1E). Cell dimensions measured from the
373 three strains were 21–45 μm long ($30.4 \pm 4.5 \mu\text{m}$, $n = 169$) and 21–46 μm wide ($31.7 \pm 4.5 \mu\text{m}$,
374 $n = 169$), with a length: width ratio of 0.7–1.2 (0.96 ± 0.07 ; $n = 169$) (Fig. 11A). The episome
375 and hyposome were almost equal in size. The cingulum was median, with a cingular width of
376 2.5–6.2 μm ($4.7 \pm 1.2 \mu\text{m}$; $n = 160$). The descending cingulum was displaced by one cingular
377 width (Fig. 2C, D, 4A). The narrow cingular lists were present along the anterior and posterior
378 sutures (Figs 1–3).

379 Cells of strain DBS08 were further examined with SEM as presented in Fig. 4. The cell
380 was covered with thin and smooth thecal plates scattered with minute pores visible in SEM (Fig.
381 4). Thecal plates formula was typical for *Alexandrium*: Po, 4', 6'', 6C, 8–10S, 5''', 2'''. The plate
382 arrangement is schematically illustrated in Fig. 5. The epitheca consisted of four apical plates (4'),
383 six precingular plates (6''), and an apical pore plate (Po) (Figs 1, 3, 4). The ventrally positioned
384 first apical plate 1' was consistently disconnected from the Po. It was pentagonal with two
385 anterior margins, the left margin touching 2' being shorter than the right margin adjoining 4'
386 (Figs 1G, I, 3A–C, 4A–D). The plate was 4.8–13.7 μm long ($9.6 \pm 1.8 \mu\text{m}$; $n = 132$) and 2.9–8.7
387 μm wide ($6.2 \pm 1.2 \mu\text{m}$; $n = 87$), with the ratio of length: width of 1.3–3.1 (1.71 ± 0.28 ; $n = 87$)
388 (Fig. 11A).

389 A large ventral pore (Vp), which was visible occasionally in LM (Fig. 2F), was usually
390 not in contact with the first apical plate 1' and was located on the suture between plates 2' and 4',
391 forming similar-sized circular indentations on the edges of the right posterior margin of 2' and

392 left anterior margin of 4'. This arrangement (Figs 1G, I, 3D) was observed for 64% of cells of
393 strain DBS08 ($n = 64$); and for 57% of cells of strain Atay99Shio-02 ($n = 77$); However, in many
394 cases, the distance between the anterior tip of plate 1' and the pore plate (i.e. the suture length of
395 2'/4') was so short that the Vp was seen almost in contact with 1' (Figs 3C, 4A, C), which was
396 the case for 36% and 43% of cells of strains DBS08 and Atay99 Shio-02, respectively. The
397 length of sutures adjoining plates 2' and 4' (i.e., the distance between 1' and Po, herein referred
398 2'/4' suture) was 1.3–5.9 μm ($3.5 \pm 1.1 \mu\text{m}$; $n = 74$), with the ratio of 2'/4' suture to 1' length
399 ranging from 0.2–0.7 (0.4 ± 0.16 ; $n = 74$) (Fig. 11A). For cells with an unusual long suture of
400 plates 2' and 4', the Vp was consistently located almost exactly halfway between the anterior tip
401 of 1' and the pore plate (Fig. 4D).

402 The Po was narrowly ovate, with a rounded dorsal and a pointed ventral end, and a hook-
403 shaped pore was visible (Figs 1G–I, 3A–C, 4A–D). No anterior attachment pore was observed.
404 The third apical plate 3' was symmetrical, positioned on the dorsal part of the epitheca (Figs 1H–
405 I, 3D, E, 4B, C). Plate 6'' was the smallest precingular plate, pentagonal, longer than wide (Figs
406 1G, I, 3A–C, J, 4A, C–E). The plate was 6.0–13.8 μm long ($9.3 \pm 1.4 \mu\text{m}$; $n = 85$) and 3.2–7.8
407 μm wide ($5.1 \pm 0.9 \mu\text{m}$; $n = 85$), with the ratio of length: width of 1.4–2.3 (1.86 ± 0.22 ; $n = 85$)
408 (Fig. 11A).

409 The sulcus was narrow and short, bordered by sulcal lists on the right margin of the first
410 postcingular plate (1''') and the first antapical plate (1''''), and the left margin of the fifth
411 postcingular plate (5''') (Fig. 4A, E). The anterior sulcal plate (Sa) was narrow (Fig. 1G, J),
412 situated almost perpendicularly below 1', and slightly invaded the epitheca (Fig. 4E). Its right
413 lateral suture adjoining the left lateral margin of 6''. Its anterior left lateral margin was a
414 continuation of the right lateral margin of 1' (Fig. 4E). In the sulcus, the following eight larger

415 plates were clearly identified: left anterior sulcal (Ssa), left posterior sulcal (Ssp), right posterior
416 sulcal (Sdp), right anterior sulcal (Sda), anterior median sulcal (Sma), and the posterior median
417 sulcal (Smp) plate (Figs 1G, I, J, 3G–I, 4E). Moreover, two small accessory sulcal plates, the
418 anterior accessory (Saca) and posterior accessory (SACP) plates were at times visible in
419 fluorescence microscopy (Fig. 1I, J). The plate Ssa was the largest (Figs 1G, I, J, 3G–I), laid
420 posteriorly to the Sa, with the anterior margin touching plate Sa, Sma, and C₁ (Figs 3H, I, 4E).
421 The plate Sdp was slender and longer than the irregular triangular Ssp (Figs 1G, I, J, 3G–I, 4E).
422 The plate Sda was triangular and had a small list covering the anterior and left margins of the
423 plate (Figs 1G, I, J, 3H, 4E). Two small median sulcal plates, Sma and Smp, were identified
424 (Figs 1I, J, 3G–I, 4E). The plate Sma was situated right below Sa (Fig. 1G, J, 3G–I) and vaulted
425 over the flagellar pore (Fig. 4E). The plate Smp located between plates Ssa and Sdp was visible
426 under epifluorescence microscopy (Fig. 1I, J, 3G–I), but this plate could not be demonstrated
427 under SEM. Two accessory plates were at times observed; Saca was triangular, and SACP was
428 irregularly quadrangular (Fig. 1I, J). The Sp was elongated, longer than wide, and slanting to the
429 posterior right (Figs 1J, 2F, G, 3G). Occasionally a line or groove on plate Sp was present (Fig.
430 3F). The W-shaped anterior margin of the plate was in contact with the sulcal plates Sdp and Ssp
431 (Figs 3F, G, I, 4G). There were six cingular plates (C₁–C₆) of almost equal size (Figs 1G, H, 3D,
432 F, G). The hypotheca comprised five postcingular plates, and two antapical plates. The first and
433 fifth postcingular plates (1^{'''} and 5^{'''}) were of comparable size and were the smallest among the
434 postcingular plates (Figs 3F, G, 4G). Plate 1^{'''} was trapezoidal, with a distinct sulcal list present
435 on the right margin of the plate; the anterior margin touching Ssa, Ssp, and 1^{'''} (Figs 1G, I, 3G–I,
436 4G). The broad pentagonal plate 2^{'''} was located at the antapical position (Figs 3F, G, 4G).
437

438 *Alexandrium ogatae* sp. nov.

439 S.T.Teng, N.Abdullah, Tillmann, Leaw et P.T.Lim

440 (Figs 6–8)

441

442 DESCRIPTION: Photosynthetic, thecate dinophyte. Cells solitary, or in two-cell chains,
443 subspherical to irregularly heptagonal in outline, 23–43 μm long, 25–48 μm wide. Rough theca
444 surface with dense pores. Cingulum median, descending one cingular width, with cingular lists
445 along anterior and posterior sutures. Thecal tabulation: Po, 4', 6'', 6C, 8–10S, 5''', 2'''''. Plate 1'
446 pentagonal, no contact with apical pore plate, left anterior margin shorter than right. Plate 6''
447 wider than long. Ventral pore absent. Small pore present on right anterior part of anterior sulcal
448 plate (Sa). Sa incised right posterior end of 1'. Left anterior and posterior lateral sulcal plates
449 (Ssa and Ssp) almost equal in size. Sulcal lists present on right margin of plates 1''', 1''''', Ssa, and
450 left margin of 5'''. Posterior sulcal plate (Sp) elongated.

451

452 HOLOTYPE: Glutaraldehyde-fixed material of strain LASpbB10 (labelled 'holotype of
453 *Alexandrium ogatae*, prepared from strain LASpbB10, Sepanggar Bay, Sabah, 15/3/2017')
454 deposited at the Aquatic Botany Culture Collection, University Malaysia Sarawak, Malaysia.

455

456 TYPE LOCALITY: Sepanggar Bay (6° 5' 29.3388" N, 116° 7' 39.2772" E), Sabah, Malaysia Borneo.

457

458 ETYMOLOGY: The species is named after Dr. Takehiko Ogata (Japan) for his contribution to the
459 research in PSP toxins and capacity development in the Southeast Asian region.

460

461 ***Alexandrium ogatae* morphology**

462 Cells of strains LASpbB10 and LASpbD3 were examined morphologically and the
463 morphometrics was measured (Table 1), but only micrographs of strain LASpbB10 were
464 presented (Figs 6, 7). Cells were solitary (Fig. 6A), or in two-cell chains (Figs 6B, C, 7C), with
465 the cell outlines subspherical to irregularly heptagonal in ventral and dorsal views (Figs 6A–C,
466 7A–D). Cell content appeared brownish orange in colour, with numerous ellipsoidal chloroplasts
467 radially distributed from the center of the cell (Fig. 6A). The nucleus was located dorsally in the
468 cingular plane (Fig. 6C); when stained with SYBR, the nucleus appeared hemi-toroidal shaped in
469 the apical view (Fig. 6D). Cells were 23–43 μm long ($32.6 \pm 4.4 \mu\text{m}$; $n = 107$) and 25–48 μm
470 wide ($32.5 \pm 4.2 \mu\text{m}$; $n = 107$), with a length: width ratio of 0.7–1.3 (1.01 ± 0.11 ; $n = 107$) (Fig.
471 11A). The episome was slightly shorter than hyposome. The cingulum was narrow and
472 excavated, $3.9 \pm 1.0 \mu\text{m}$ wide (2.3–6.3 μm ; $n = 160$). The descending cingulum was displaced by
473 one cingular width and covered with cingular lists along the anterior and posterior sutures (Fig.
474 7).

475 The cell was covered with thin thecal plates, rough with noticeable numerous pores
476 scattered on the thecal plates (Fig. 7). Staining of thecal plates revealed the plate formula: Po, 4',
477 6'', 6C, 8–10S, 5''', 2'''''. The plate arrangement is schematically illustrated in Fig. 8. The epitheca
478 consisted of four apical plates, six precingular plates, and an apical pore plate (Po) (Figs 6–8).
479 The ventrally positioned first apical plate 1' was consistently disconnected from the Po,
480 pentagonal in shape, with the left margin touching 2' being shorter than the right margin
481 adjoining 4' (Figs 6F, I, K, L, 7A–C, E, F). The length of plate 1' was 7.0–15.9 μm (10.7 ± 2.0
482 μm ; $n = 107$), and the width of 4.0–11.8 μm ($7.6 \pm 1.6 \mu\text{m}$; $n = 61$), with a ratio of length: width
483 of 1.1–2.0 (1.44 ± 0.18 ; $n = 61$). There was no Vp in the specimens examined ($n = 107$). The

484 length of the suture between plates 2' and 4' (herein referred 2'/4' suture) was 2.7–7.9 μm ($4.9 \pm$
485 $1.5 \mu\text{m}$; $n = 46$), with the ratio of 2'/4' suture to 1' length ranging from 0.3–0.6 (0.46 ± 0.08 ; $n =$
486 46). The Po was ovate to irregularly triangular, with a slightly straight dorsal margin, and a
487 hook-shaped pore was visible in the middle of the plate (Fig. 6F, K). In some cells, a large
488 anterior attachment pore (aap) was seen located between the right margin of Po and 4' (Figs 6F,
489 7E, F). The apical plates 2', 3', and 4' surrounding the Po were almost equal in size; plates 3' and
490 4' were symmetrical. Plate 6'' was pentagonal, usually longer than wide (Figs 6I, L, 7C). The
491 plate was 5.6–12.4 μm long ($8.7 \pm 1.7 \mu\text{m}$; $n = 61$) and 3.2–11.4 μm wide ($6.9 \pm 2.1 \mu\text{m}$; $n = 61$),
492 with the ratio of length: width of 0.9–2.3 (1.34 ± 0.39 ; $n = 61$) (Fig. 11A).

493 The sulcus was broad and shallow, slightly extending into the epitheca. It was bordered
494 by sulcal lists on the right margins of the first postcingular (1'''), the first antapical (1''''), the
495 anterior sulcal plate (Ssa), and on the left margin of the fifth postcingular plate (5'''). In addition,
496 there were short lists on the posterior margin of 1' and the left posterior margin of 6'' (Fig. 7A–
497 C). In the sulcal area, the left anterior sulcal (Ssa), left posterior sulcal (Ssp), right posterior
498 sulcal (Sdp), right anterior sulcal (Sda), anterior median sulcal (Sma), and posterior median
499 sulcal (Smp) plates (Figs 6I, K, L, N, 7A–C), and two accessory plates, anterior and posterior
500 accessory (Saca, Sacp), were seen in fluorescence microscopy (Fig. 6I, K, L, N). Plate Ssa was
501 located directly posterior to the first cingular plate (C_1) (Fig. 7A–C). The plate Sa was irregularly
502 A-shaped. A pore was situated on the right anterior part of the plate (Figs 6I, K, L, 7A, C); when
503 observed on the dissected plates, it appeared as a circular incise on the edge of the plate (Fig. 6I,
504 K, L). Plate Ssp was comparable in size to Ssa, irregularly pentagonal in shape (Fig. 6G–I, K, L,
505 N). Plate Sdp was elongated (Figs 6G, K, L, N, 7A, C). Plate Sda was triangular and had a small
506 list covering the anterior and left margins of the plate (Figs 6G, I, K, L, N, 7A–C). Two small

507 central median sulcal plates, Sma and Smp, were identified from fluorescence microscopy (Fig.
508 6I, K, L, N). The plate Sma was located next to the left posterior end of Sa and adjoined Ssa (Fig.
509 7A, C). Plate Smp and the two tiny accessory plates, Saca and Sacp, were observed in LM but
510 not in SEM. The Saca was long, oblique triangular, Sacp was the smallest sulcal plates (Fig. 6I,
511 K, L, N).

512 The hypotheca comprised five postcingular plates and two antapical plates. Plate 4''' was
513 the largest among the postcingular plates (Figs 6G, H, 7G). Plate 1'''' was irregularly triangular,
514 with a clear sulcal list present on the right suture of the plate (Figs 7G, H). The Sp was elongated,
515 longer than wide, with an obliquely V-shaped anterior margin (Figs 6G, H, N, 7G, H). In some
516 cells, a relatively large irregular oval posterior attachment pore (pap) was observed on the right
517 side of Sp (Figs 6G, M, N, 7H). Plate 2'''' was pentagonal, slightly longer than wide (Figs 6G, H,
518 7G), located at the antapex, and positioned obliquely to the left ventral side of the cell (Fig. 7A,
519 G).

520

521 *Alexandrium pseudogonyaulax* morphology

522 Cells of *A. pseudogonyaulax* strains LMIAE9 and LATAG8 were subspherical and
523 ranged from 21–42 μm in length ($31.2 \pm 4.8 \mu\text{m}$; $n = 66$) and 24–45 μm in width ($33.3 \pm 5.0 \mu\text{m}$;
524 $n = 66$) in size. The length: width ratio of 0.8–1.4 (0.94 ± 0.09 ; $n = 66$) (Fig. 11A) was quite
525 variable with some cells being longer than wide (Fig. 9A–C) or wider than long (Fig. 9I). The
526 nucleus was located in the cingular plane, with both ends visible in the ventral view under LM
527 (Fig. 9A–C); when stained with SYBR, the nucleus appears hemi-toroidal shaped in the apical
528 view (Fig. 9D). The cells were brownish orange in colour, with numerous granular chloroplasts

529 visible under light (Fig. 9A–C) and fluorescence microscopy (Fig. 9E). The cingulum was
530 narrow, displaced by approximately one cingular width (Fig. 9I).

531 The theca was composed of thin and smooth plates. Thecal plates were with typical
532 *Alexandrium* plate tabulation: Po, 4', 6'', 6C, 8–10S, 5''', 2'''' (Fig. 9F–K). Plate 1' was
533 pentagonal, disconnected from Po, with a shorter left anterior margin (Fig. 9F, I, J). Occasionally,
534 cells with a quadrangular 1' plate were observed (Fig. 9G). Plate 1' was 5.4–12.9 μm long ($9.5 \pm$
535 $1.8 \mu\text{m}$; $n = 62$) and 4.0–9.5 μm wide ($7.0 \pm 1.3 \mu\text{m}$; $n = 40$), with the length: width ratio ranging
536 from 1.2 to 1.7 (1.43 ± 0.13 ; $n = 40$). The Po was surrounded by plates 2', 3', and 4'. A large
537 ventral pore (Vp) was observed in the midpoint of the suture between 1' and 4' (Fig. 9F–G, I, J).
538 The 2'/4' suture length was 3.0–7.8 μm ($4.7 \pm 1.2 \mu\text{m}$; $n = 22$); the ratio of 2'/4' suture: 1' length
539 was 0.4–0.7 (0.53 ± 0.07 ; $n = 22$). Plate 6'' was pentagonal, slightly longer than wide (Fig. 9F–G,
540 I); 6.1–13.9 μm long ($9.3 \pm 1.7 \mu\text{m}$; $n = 40$) and 3.9–10.6 μm wide ($6.4 \pm 1.4 \mu\text{m}$; $n = 40$), with
541 the length: width ratio of 1.2–1.9 (1.48 ± 0.18 ; $n = 40$) (Fig. 11A). Plate Ssa was large and wide
542 (Fig. 9F, H). The accessory sulcal plates, Saca and Sacp, were observed (Fig. 9F, H). Plate Sp
543 was elongated and oblique to the right (Fig. 9G, K). Plate 2'''' was wider than long (Fig. 9K).

544

545 ***Alexandrium taylorii* morphology**

546 Cells of *A. taylorii* strains AY7T and AY1T from the Adriatic Sea agreed largely with the
547 original species description in Balech (1994). The thecal examination of the strain AY7T was
548 presented in detail in Tillmann *et al.* (2020), and AY1T is presented here in Fig. 10. Thecal plate
549 morphometric measurements were made on both strains for comparison (Fig. 11A).

550 Cells were solitary (Fig. 10A–D), but doublets were observed shortly after cell division
551 (Fig. 10E). Cells were subspherical to irregularly hexagonal in outline (Fig. 10A–G) and 27–48

552 μm long ($38.2 \pm 4.6 \mu\text{m}$; $n = 102$) and 27–49 μm wide ($39.4 \pm 4.9 \mu\text{m}$; $n = 102$), with the length:
553 width ratio of 0.9–1.1 (0.97 ± 0.04 ; $n = 102$). The cingulum was narrow and displaced by about
554 one cingulum width (Fig. 10G, H). The plate tabulation was determined as Po, 4', 6'', 6C, 8S, 5''',
555 2'''' (Fig. 10H–O). Plate Po was disconnected from the pentagonal to quadrangular 1' (Fig. 10H–
556 L, N–O). A large Vp was present above 1' and was located in the junction of plates 1', 2', and 4'
557 (Fig. 10H–K, N). In the cultured material of strain AY1T there was some slight variability in the
558 position of the Vp. In one out of 58 cells examined (2%), the Vp was located on the suture
559 between plates 2' and 4' (not shown). Exceptional deviation in Vp position was also observed for
560 the cultured cells of strain AY7T, where three of 75 examined cells (4%) had a Vp located on the
561 suture of plates 2' and 4' (see Supplementary Figure 1E, L, O in Tillmann et al., 2020). Moreover,
562 for this strain, among the 75 cells examined in detail, one cell lacking an obvious Vp and one cell
563 with two ventral pores (see Supplementary Figure 1S and 1T in Tillmann et al., 2020) were
564 present. The length and width of 1' were 8.8–14.6 μm ($11.0 \pm 1.0 \mu\text{m}$; $n = 100$) and 6.6–10.4 μm
565 ($8.5 \pm 0.8 \mu\text{m}$; $n = 100$), respectively; with the ratio of length: width of 1' ranging from 1.0 to 1.6
566 (1.31 ± 0.12 ; $n = 100$). The 2'/4' suture length was 4.8–12.0 μm ($7.3 \pm 1.3 \mu\text{m}$; $n = 85$). The ratio
567 of 2'/4' suture: 1' length was 0.5–0.9 (0.66 ± 0.09 ; $n = 85$). Plate 6' was irregularly pentagonal
568 and longer than wide (Fig. 10H–O). Dimensions of plate 6' were 9.0–15.6 μm in length ($10.8 \pm$
569 $1.0 \mu\text{m}$; $n = 91$) and 5.8–12.3 μm in width ($7.5 \pm 1.0 \mu\text{m}$; $n = 91$), with a ratio of 6' length: width
570 of 1.1–1.9 (1.46 ± 0.14 ; $n = 91$) (Fig. 11A).

571 In the sulcal area, plate Sa extended into the epitheca. This plate was narrow and not in
572 contact with the first precingular plate (Fig. 10H, J). The posterior sulcal plate was elongated and
573 at times had a conspicuous line or groove (Fig. 10O). The left sulcal plate was large (Fig. 10N,

574 O) and the central sulcal area consisted of plates Sma, Smp, Ssp, Sda, and Sdp (Fig. 10O).

575 Additional accessory sulcal plates were not observed.

576

577 **3.2. Morphometric comparisons**

578 The individual and variable plots of the morphometric data for the first (Dim1) and
579 second (Dim2) principal components are shown in Fig. 11B. These first two dimensions express
580 91% of the total inertia; of which Dim1 accounts for 55% of the variation, while Dim2 for 36%.
581 The total inertia was strongly greater than the reference value (22%), the variability explained by
582 this plane is thus highly significant (Wilks test, $p < 0.0001$).

583 The first principal component (Dim1) has large positive associations with the ratio of
584 2'/4' suture:1' length, 2'/4' suture length, and width of 6'', indicating informative descriptors of
585 these traits. The dimension distributed cells of *A. taylorii* toward the positive values of Dim1,
586 characterized by higher values for the ratio of 2'/4' suture:1' length, 2'/4' suture length, and the
587 width of 6'', separating them from other species. Whilst cells of *A. limii* were separated from *A.*
588 *taylorii*, *A. ogatae*, and *A. pseudogonyaulax*, attributed to higher values for length: width ratio of
589 1', cell length: width ratio, and length: width ratio of 6'' (Fig. 11B).

590

591 **3.3. Molecular characterization**

592 **3.3.1. rDNA sequence information and phylogenetic inference**

593 Nucleotide sequences of three nuclear-encoded rDNA (SSU, LSU D1-D3, and ITS) of
594 *Alexandrium* species in this study were obtained to address species delineation. The newly
595 obtained sequences of each *Alexandrium* strain and those retrieved from the GenBank nucleotide
596 database are given in Table S1. Phylogenetic analyses of the three markers yielded identical tree

597 topologies by MP, ML, and BI, with the BI trees shown for LSU, SSU, and ITS1-5.8S-ITS2
598 markers (Fig. 12, Figs S1–S3). While for the ITS2 sequence-structure tree reconstruction, the
599 ML tree is presented (Fig. 12).

600 The SSU rDNA multiple alignments of 112 taxa yielded 1655 characters, of which 656
601 were parsimony-informative, 78 were parsimony-uninformative, and 921 were constant. The
602 LSU dataset of 108 taxa yielded a final alignment of 822 characters (555 were parsimony-
603 informative, 57 were parsimony-uninformative, and 210 characters were constant). The ITS
604 dataset yielded an alignment of 622 characters (549 were parsimony-informative, 12 were
605 parsimony-uninformative, and 61 characters were constant). The phylogenetic reconstructions
606 from these datasets are presented in Supplementary Figs S1–S3.

607 The trees showed a consistent monophyletic grouping of *A. limii*, *A. ogatae*, *A. taylorii*,
608 and *A. pseudogonyaulax* (Fig. 12). In the LSU and ITS1-5.8S-ITS2 trees, *A. limii* formed a sister
609 clade with *A. pseudogonyaulax*. In the SSU tree, it formed a sister clade with *A. taylorii*.
610 *Alexandrium ogatae* consistently made up a basal node to *A. limii*, *A. taylorii*, and *A.*
611 *pseudogonyaulax*, with strong nodal supports in both SSU and LSU trees (Fig. 12). In the ITS1-
612 5.8S-ITS2 tree, it formed a sister clade to (*A. limii*+*A. pseudogonyaulax*). While the ITS2
613 sequence-structure tree revealed the sister relationship with *A. limii* (Fig. 12).

614 The pairwise sequence divergences (uncorrected *p*-distance) for *A. limii*, compared to its
615 close relatives, ranged from 0.3–1.6% for the SSU dataset (Table S10), 4.2–13.4% for the LSU
616 dataset (Table S11), and 23.2–24% for the ITS1-5.8S-ITS2 dataset (Table S12). While the
617 pairwise uncorrected *p*-distances of *A. ogatae* to its close relatives ranged from 1.5–2% for the
618 SSU dataset (Table S10), 12.3–13.9% for the LSU dataset (Table S11), and 15.3–18.5% for the
619 ITS1-5.8S-ITS2 dataset (Table S12).

620

621 **3.3.2. ITS2 sequence-structure information**

622 The ITS2 secondary structures of *A. limii*, *A. ogatae*, *A. taylorii*, and *A. pseudogonyaulax*
623 revealed the core features of the ITS2 transcript, with four common helices. Pairwise structural
624 comparison of the ITS2 RNA transcripts between *A. limii* (Fig. 13A) and *A. ogatae* (Fig. 13B)
625 revealed one CBC in Helix II (A-U↔G-C) and six HCBCs (Fig. 13C). When comparing with *A.*
626 *pseudogonyaulax*, no CBC but six HCBCs were detected: two in Helix I (G-U↔G-C; U-
627 A↔UG), one in Helix II (U-A↔U-G), two in Helix III (G-C↔G-U; U-G↔C-G) and one in
628 Helix IV (U-G↔C-G). The pairwise comparison of *A. limii* and *A. taylorii* revealed no CBC but
629 three HCBCs: one in Helix I (G-U↔G-C) and two in Helix IV (G-U↔A-U; U-G↔C-G). The
630 pairwise comparison of the ITS2 transcript of *A. ogatae* (Fig. 13B) with its close relatives
631 showed two CBCs (in Helix III, A-U↔G-C; C-G↔U-A) and eight HCBCs for *A.*
632 *pseudogonyaulax*; and five HCBCs for *A. taylorii* (Fig. 13C).

633

634 **3.3. Toxin profiles**

635 Two strains each of *A. taylorii*, *A. limii*, and *A. ogatae* (Table 2) were analyzed for toxins
636 associated with the genus *Alexandrium*, namely PSTs, gymnodimines and spirolides (both
637 belonging to the group of cycloimines), and goniodomins (GDs). None of the strains contained
638 detectable levels of PSTs and cycloimines (for detection limits, see Tables S2, S3), but all strains
639 contained GDs (Table 2). Both *A. taylorii* and *A. ogatae* strains contained GDA as major GD
640 variants in the range between 6.3 and 13.7 pg cell⁻¹, and this was also true for the *A. limii* strain
641 DBS08 isolated at the coast of Borneo, with a cell quota of 12.9 pg cell⁻¹. In contrast, the *A. limii*
642 strain Atay99Shio-02 from Japan did not contain GDA, but a desmethyl variant of GDA. The

643 cell quota of this putatively 34-desmethyl-GDA was determined on three independently grown
644 subcultures and varied from 1.4 to 7.3 pg cell⁻¹. Also, *A. taylorii* strain AY1T contained a
645 desmethyl variant of GDA as a minor component at a cell quota of 0.6 pg cell⁻¹, but clearly not
646 the putative 34-desmethyl-GDA of *A. limii* strain AtayShio99-02. The collision-induced
647 dissociation (CID) spectrum of this compound strongly suggests a 9-desmethyl configuration of
648 GDA (data not shown). Detailed information on the structural characteristics of the GDA
649 desmethyl variants will be reported elsewhere.

650

651 **4. Discussion**

652 **4.1. Comparison of new species with their closely related species**

653 *Alexandrium limii* is morphologically and genetically closer to *A. taylorii*, and this
654 explains that some Pacific strains previously identified as *A. taylorii*, in fact, represent the new
655 species *A. limii*. This refers to the Japanese strains (included in the present study) and the *A.*
656 *taylorii* strain described by Lim et al. (2005), which we here also can reassign as *A. limii* after
657 thorough morphological observations of the field specimens from the same location and
658 comparison with clonal cultures. Both *A. taylorii* and *A. limii* share a longer-than-wide
659 pentagonal plate 1' (Balech, 1995; Tillmann et al., 2020; this study), with the left posterior
660 margin touching C₁ (Tillman et al., 2020). Nonetheless, both species are readily distinguishable
661 by the plate and morphometric differences as examined in this study. *Alexandrium limii* is
662 slightly smaller compared to *A. taylorii*. More importantly, the 2'/4' suture length in relation to
663 the length of plate 1' is shorter in *A. limii* when compared to that of *A. taylorii*; and plates 1' and
664 6'' are relatively narrower in *A. limii*, with larger length: width ratios (Fig. 11A). Morphometrics
665 multivariate comparison by PCA further supported the separation of the two species (Fig. 11B).

666 They are also distinguishable by the position of Vp. The Vp of *A. limii* is located on the suture
667 between 2' and 4' forming circular indentations on the edges of the plates. However, when the
668 suture length of 2' and 4' is short, this can be difficult to observe and the Vp is located very close
669 to the junction of 1', 2' and 4'. The Vp of *A. taylorii* is usually located in the confluence point of
670 either 1' and 4' or 1', 2', and 4' (Balech, 1995; Tillmann et al., 2020), although it must be noted
671 that in the cultured material, rare exceptions of cells with a Vp disconnected from plate 1' and
672 located on the 2'/4' suture were also observed. Complementary studies on the Vp position of field
673 samples are needed to finally evaluate if such rare deviation of Vp position can be explained by
674 culture artifacts. While the morphological trait of the presence/absence of Vp in *Alexandrium* has
675 been regarded as taxonomic uninformative (Hansen et al., 2003) the presence/absence of Vp of
676 the species examined in this study (disregarding the single cell of *A. taylorii* strain AY7T, for
677 which no vp could be identified, see Suppl. Figure 1S in Tillmann et al. 2020) was stable intra-
678 specifically.

679 With its metasert plate 1' and lacking a Vp, *A. ogatae* is different from almost all other
680 *Alexandrium*. The only similar species is *A. foedum* (Balech, 1990); which also lacks a Vp and
681 has a small notch located on the right or middle part of the anterior margin of Sa. The species,
682 however, differ from *A. foedum* originally described by Balech from the Gulf of Salerno, Italy
683 (37–48.5 µm long, 40–53 µm wide; Balech, 1990) by having a smaller cell size range (23–43 µm
684 long, 25–48 µm wide). Furthermore, the left and right lateral margins of 1' are almost parallel in
685 *A. ogatae* (Fig. 7A–C, E), whereas they are non-parallel in *A. foedum* causing the posterior part
686 of 1' to be narrow (Balech, 1990). Plate 3' of *A. ogatae* is symmetrical (Fig. 6G, 7F) but the plate
687 is asymmetrical in *A. foedum* (Balech, 1990). The cingulum of *A. ogatae* is descending by about
688 one cingular width but in *A. foedum* it is usually less than one cingular width (0.5–0.75; Balech,

689 1990). Genetically, *A. ogatae* singled out and formed a strong basal node to *A. limii*, *A.*
690 *pseudogonyaulax*+*A. hiranoi*, and *A. taylorii* in the SSU and LSU trees (Fig. 12). However, no
691 molecular data on *A. foedum* is currently available to assess if the two species are indeed the
692 closest. It is noteworthy that Ssa of *A. ogatae* is particularly superficial (not inside the sulcus)
693 and look as though a precingular than a sulcal plate.

694 The two new species readily differ from *A. pseudogonyaulax* by the position of Vp,
695 where the Vp of *A. pseudogonyaulax* is consistently located on the suture between 1' and 4'.
696 Cells of *A. pseudogonyaulax* examined in this study (Fig. 9) largely conform with the original
697 description of *A. pseudogonyaulax* (Biecheler, 1952), with slight differences in the cell shape.
698 *Alexandrium pseudogonyaulax* described by Biecheler (1952) is explicitly compressed (wider
699 than long) (Balech, 1995). However, cells with both a compressed form and a slightly longer-
700 than-wide cell shape were observed in this study. Also, cells of *A. pseudogonyaulax* from Danish
701 waters were reported to exhibit large variability in cell shape (Kremp et al., 2019). Nonetheless,
702 these cell shape characters have been used to differentiate between *A. pseudogonyaulax* and *A.*
703 *hiranoi*, where *A. hiranoi* is described with a longer-than-wide cell shape (Kita and Fukuyo,
704 1988; Balech, 1995). It is interesting to note that both species are genetically closer, this is
705 supported by the sequence of *A. hiranoi* NIES-612 strain from the type locality (Jogashima
706 Island, Japan) being recovered as a sister taxon in the LSU tree with strong nodal supports (Kim
707 et al., 2005; Fig. S2). Cell shape is likely not a good diagnostic feature to distinguish between the
708 two species, but according to the literature (Kita and Fukuyo, 1988; Balech, 1995) they are
709 additionally differentiated by the position of Vp and the shape of 1'.

710

711 4.2. Species concepts in subgenus *Gessnerium*

712 The present study confirms previous phylogenetic studies indicating that the
713 morphological concept of Balech (Balech, 1995), considering a metasert or exsert first apical
714 plate (1') without clear contact to the pore plate (Po) as a synapomorphy of *Gessnerium*, a
715 subgenus of *Alexandrium*, failed. Three of Balech's *Gessnerium* species, i.e., *A. insuetum*, *A.*
716 *margalefii*, and *A. pohangense* in the present and many previous phylogenetic studies were
717 unrelated to other *Gessnerium* species and grouped with species of the subgenus *Alexandrium*
718 *sensu* Balech (Balech, 1995). While both *A. margalefii* and *A. pohangense* clustered next to each
719 other in a well-supported clade with *A. leei*, *A. insuetum* is quite distantly embedded in the
720 cluster of *A. minutum*, *A. tamutum*, and the allied species, and this again underlines the
721 paraphyletic nature of a metasert/exsert 1' plate. The question now arises if there are
722 morphological features unifying all species of the molecularly defined *Gessnerium* clade. In a
723 first attempt, a dichotomous identification scheme was constructed which enables species
724 differentiation of those species of Balech's morphological *Gessnerium* concept (Fig. 14). By
725 using morphometry of plate Sp, this tree indicates that the three "outlier" species (*A. insuetum*, *A.*
726 *margalefii*, and *A. pohangense*) do not share the elongated and oblique Sp, which is typical for
727 most species of the molecularly defined *Gessnerium* clade. The *Gessnerium* clade species *A.*
728 *monilatum* and *A. satoanum* also do not have an elongated oblique Sp, but their Sp is broad and
729 thus different from those of *A. insuetum* (Sp wider than long) and *A. margalefii/A. pohangense*
730 (Sp longer than wide). The shape of the Sp plate of *A. globosum* is very similar to that of *A.*
731 *margalefii* and *A. pohangense*, suggesting that this species probably is not included in the
732 molecularly defined *Gessnerium* clade. The same likely refers to *A. concavum* and *A.*
733 *camurascutulum*, whose Sp plate is similar in shape to the Sp of *A. insuetum*. Based on Fig. 14 it
734 may be concluded that *A. balechii*, *A. foedum* (species of Balech's *Gessnerium*, but no molecular

735 data available yet), with their elongated oblique Sp, are likely also members of the molecularly
736 defined *Gessnerium* clade. However, more efforts are needed to obtain sequence data of these
737 up-to-now poorly known species of *Alexandrium* to clarify their phylogenetic position.

738

739 **4.3. GD-producing *Alexandrium* species**

740 With the description of *A. limii* and *A. ogatae* as new and GD-producing species, the
741 number of GD-producing species of *Alexandrium* has increased to six, adding *A. limii* and *A.*
742 *ogatae* to the already known GD producers *A. monilatum*, *A. hiranoi*, *A. pseudogonyaulax*, and *A.*
743 *taylorii* (Tillmann et al., 2020). Thus, the production of GD seems to be a common trait, i.e. a
744 chemical synapo”morphie” for all the species of the molecularly defined *Gessnerium* clade of
745 *Alexandrium*. Only one of the species in this clade, *A. satoanum*, has not been tested yet for the
746 presence of GD, likely because no cultured strains are currently available. Likewise, it would be
747 interesting to grow and test other strains with a *Gessnerium*-type 1’ configuration but of
748 unknown phylogenetical position, i.e., *A. balechii*, *A. concavum*, *A. camurusculatum*, *A. foedum*
749 and *A. globosum* for the presence of GD. In any case, almost all species and strains of the
750 *Gessnerium* clade reported to date produce GDA as the major component of the GD profiles. The
751 most notable exception by now is the Japanese *A. limii* strain Atay99Shio-02 which produced
752 exclusively a desmethyl variant of GDA, most likely 34-desmethyl-GDA, at a cell quota
753 comparable to GDA of the other strains. Desmethyl variants have been reported before in
754 planktonic field samples of the Danish Limfjord and in 11 out of 17 clonal strains of *A.*
755 *pseudogonyaulax* isolated from this area (Krock et al., 2018), erroneously reported as GDB
756 (Harris et al., 2021). The same compound is reported here for *A. taylorii* strain AY1T from the
757 Mediterranean (Table 2). However, the desmethyl variants of all these strains are putatively 9-

758 desmethyl-GDA and were only produced as minor compounds besides GDA. Due to the low
759 number of available GD-producing strains, it is still impossible to say, if these differences in GD
760 profiles are associated with certain species and/or geographic patterns. It is interesting to note
761 that all of the GD-producing strains do not produce PSTs (Krock et al., 2018; Tillmann et al.,
762 2020; this study). However, one strain (reported as *A. taylorii*, reassigned here as *A. limii*) was
763 reported to contain extremely low cellular contents of <1 fmole cell⁻¹ by HPLC (Lim et al., 2005),
764 which is in need of analytical confirmation by LC/MS-MS.

765

766 **5. Conclusion**

767 Two novel *Alexandrium* species were described based on both morphology and
768 molecular evidence, hereby the names *Alexandrium limii* sp. nov. and *A. ogatae* sp. nov. were
769 proposed. Both new species were shown to produce GDA, and this is the first report of the
770 occurrence of GD-producing *Alexandrium* species in the Southeast Asian region. Although there
771 is no evidence of human intoxication nor cases of GD contamination reported in the Western
772 Pacific, GD analyses should be included in routine toxin monitoring and shellfish sanitation
773 programs in the region as a proactive measure to safeguard human health and seafood safety.

774

775 **Acknowledgments**

776 The work was supported by the Ministry of Higher Education, Malaysia, Higher Institution
777 Centers of Excellence Grant [HICoE IOES-2023B] and Long-term Research Grant Scheme
778 (LRGS) [LRGS/1/2020/UMT/01/1/3] to P.T. Lim, and by the PACES II research program of the
779 Alfred-Wegener-Institute (AWI) as part of the Helmholtz Foundation initiative in Earth and
780 Environment. Special thanks to Thomas Max and Anne Müller (both AWI Bremerhaven,

781 Germany) for their continued support in toxin analysis. This forms part of the master project of
782 N. Abdullah.

783 **References**

- 784 Anderson, D. M., Alpermann, T. J., Cembella, A. D., Collos, Y., Masseret, E., & Montresor, M.,
785 2012. The globally distributed genus *Alexandrium*: multifaceted roles in marine
786 ecosystems and impacts on human health. *Harmful Algae* 14, 10–35.
787 doi:10.1016/j.hal.2011.10.012.
- 788 Ankenbrand, M. J., Keller, A., Wolf, M., Schultz, J., Förster F., 2015. ITS2 database V: Twice as
789 much. *Mol. Biol. Evol.* 32, 3030–3032. doi:10.1093/molbev/msv174
- 790 Balech, E., 1995. The genus *Alexandrium* Halim (Dinoflagellata). Sherkin Island Marine Station
791 Publication, Sherkin Island, Co. Cork, Ireland.
- 792 Biecheler, B., 1952. Recherches sur les Péridiniens. *Bull. Biol. France Belg.* 36 (Suppl), 1–149.
- 793 Branco, S., Oliveira, M. M., Salgueiro, F., Vilar, M. C., Azevedo, S. M., Menezes, M., 2020.
794 Morphology and molecular phylogeny of a new PST-producing dinoflagellate species:
795 *Alexandrium fragae* sp. nov. (Gonyaulacales, Dinophyceae). *Harmful Algae* 95, 101793.
- 796 Coleman, A. W., 2009. Is there a molecular key to the level of “biological species” in
797 eukaryotes? A DNA guide. *Mol. Phylogenet. Evol.* 50(1), 197–203.
- 798 [Condie, S.A., Oliver, E.C.J., Hallegraeff, G.M., 2019. Environmental drivers of unprecedented](#)
799 [Alexandrium catenella](#) dinoflagellate blooms off eastern Tasmania, 2012–2018. *Harmful*
800 [Algae](#) 87, 101628.
- 801 Díaz, P.A., Álvarez, G., Varela, D., Pérez-Santos, I., Díaz, M., Molinet, C., Seguel, M.,
802 Aguilera-Belmonte, A., Guzmán, L., Uribe, E., 2019. Impacts of harmful algal blooms on
803 the aquaculture industry: Chile as a case study. *Perspect. Phycol.* 6, 39–50.
- 804 Darriba, D., Posada, D., 2014. jModelTest 2.0 Manual v0.1.1.

- 805 Darty, K., Denise, A., Ponty, Y., 2009. VARNA: Interactive drawing and editing of the RNA
806 secondary structure. *Bioinformatics* 25(15), 1974.
- 807 Delgado, M., Garcés, E., Vila, M., Camp, J., 1997. Morphological variability in three
808 populations of the dinoflagellate *Alexandrium taylori*. *J. Plank. Res.* 19(6), 749757.
- 809 Espiña, B., E. Cagide, M. C. Louzao, N. Vilariño, M. R. Vieytes, Y. Takeda, Sasaki, M., Botan,
810 L.M., 2016. Cytotoxicity of goniodomin A and B in non contractile cells. *Toxicology*
811 *Letters* 250–251, 10–20.
- 812 Hallegraeff, G. M., 1993. A review of harmful algal blooms and their apparent global
813 increase. *Phycologia* 32(2), 79–99.
- 814 Hansen, G., Daugbjerg, N., Franco, J. M., 2003. Morphology, toxin composition and LSU rDNA
815 phylogeny of *Alexandrium minutum* (Dinophyceae) from Denmark, with some
816 morphological observations on other European strains. *Harmful Algae* 2(4), 317–335.
- 817 Harding, J.M., Mann, R., Moeller, P.D.R., Hsia, M.H., 2009. Mortality of the veined rapa whelk,
818 *Rapana venosa*, in relation to a bloom of *Alexandrium monilatum* in the York River,
819 United States. *J. Shellfish Res.* 28, 363–367.
- 820 Harris, C.M., Krock, B., Tillmann, U., Tainter, C.J., Stec, D.F., Andersen, A.J.C., Larsen, T.O.,
821 Reece, K.S., Harris, T.M., 2021. Alkali metal and acid-catalyzed interconversion of
822 goniodomin A with congeners B and C. *J. Nat. Prod.* 84, 2554–2567.
- 823 Hsia, M.H., Morton, S.L., Smith, L.L., Beauchesne, K.R., Muncik, K.M., Moeller, P.D.R., 2006.
824 Production of goniodomin A by the planktonic, chain-forming dinoflagellate
825 *Alexandrium monilatum* (Howell) Balech isolated from the Gulf Coast of the United
826 States. *Harmful Algae* 5, 290–299.

- 827 Jin, D., Thunberg, E., Hoagland, P., 2008. Economic impact of the 2005 red tide event on
828 commercial shellfish fisheries in New England. *Ocean & Coastal Management* 51, 420–
829 429.
- 830 John, U., Litaker, R. W., Montresor, M., Murray, S., Brosnahan, M. L., Anderson, D. M., 2014.
831 Formal revision of the *Alexandrium tamarense* species complex (Dinophyceae)
832 taxonomy: the introduction of five species with emphasis on molecular-based (rDNA)
833 classification. *Protist* 165(6), 779–804.
- 834 Keller, A., Schleicher, T., Schultz, J., Müller, T., Dandekar, T., Wolf, M., 2009. 5.8S-28S rRNA
835 interaction and HMM-based ITS2 annotation. *Gene*, 430, 50–57.
- 836 Kremp, A., Tahvanainen, P., Litaker, W., Krock, B., Suikkanen, S., Leaw, C. P., Tomas, C.,
837 2014. Phylogenetic relationships, morphological variation, and toxin patterns in the
838 *Alexandrium ostenfeldii* (Dinophyceae) complex: implications for species boundaries and
839 identities. *J. Phycol.* 50, 81–100.
- 840 Kremp, A., Hansen, P. J., Tillmann, U., Savela, H., Suikkanen, S., Voß, D., Barrera, F., Jakobsen,
841 H. H., Krock, B., 2019. Distributions of three *Alexandrium* species and their toxins across
842 a salinity gradient suggest an increasing impact of GDA producing *A. pseudogonyaulax*
843 in shallow brackish waters of Northern Europe. *Harmful Algae* 87, 101622.
- 844 Krock, B., Tillmann, U., Wen, Y., Hansen, P.J., Larsen, T.O., Andersen, A.J.C., 2018.
845 Development of a LC-MS/MS method for the quantification of goniodomins A and B and
846 its application to *Alexandrium pseudogonyaulax* strains and plankton field samples of
847 Danish coastal waters. *Toxicon* 155, 51–60.
- 848 Lê, S., Josse, J., Husson, F., 2008. FactoMineR: An R Package for multivariate analysis. *J. Stat.*
849 *Software* 25(1), 1–18.

- 850 Leaw, C. P., Lim, P. T., Ng, B. K., Cheah, M. Y., Ahmad, A., Usup, G., 2005. Phylogenetic
851 analysis of *Alexandrium* species and *Pyrodinium bahamense* (Dinophyceae) based on
852 theca morphology and nuclear ribosomal gene sequence. *Phycologia* 44(5), 550–565.
- 853 Leaw, C. P., Tan, T. H., Lim, H. C., Teng, S. T., Yong, H. L., Smith, K. F., Rhodes, L., Wolf, M.,
854 Hollack, W. C., Vandersea, M.W., Litaker, R. W., Tester, P. A., Gu, H., Usup, G., Lim, P.
855 T., 2016. New scenario for speciation in the benthic dinoflagellate genus *Coolia*
856 (Dinophyceae). *Harmful Algae* 55, 137–149.
- 857 Lilly, E. L., Halanych, K. M., Anderson, D. M., 2007. Species boundaries and global
858 biogeography of the *Alexandrium tamarense* complex (Dinophyceae). *J. Phycol.* 43(6),
859 1329–1338.
- 860 Lim, H. C., Leaw, C. P., Su, S. N. P., Teng, S. T., Usup, G., Mohammad- Noor, N., Lundholm,
861 N., Kotaki, Y., Lim, P. T., 2012. Morphology and molecular characterization of
862 *Pseudo-nitzschia* (Bacillariophyceae) from Malaysian Borneo, including the new
863 species *Pseudo-nitzschia circumpora* sp. nov. *J. Phycol.* 48(5), 1232–1247.
- 864 Lim, H. C., Teng, S. T., Leaw, C. P., Lim, P. T., 2013. Three novel species in the
865 *Pseudo-nitzschia pseudodelicatissima* complex: *P. batesiana* sp. nov., *P. lundholmiae* sp.
866 nov., and *P. fukuyoi* sp. nov. (Bacillariophyceae) from the Strait of Malacca, Malaysia. *J.*
867 *Phycol.* 49(5), 902–916.
- 868 Lim, P. T., Usup, G., Leaw, C. P., 2012. Harmful algal blooms in Malaysian waters. *Sains*
869 *Malaysiana* 41(12), 1509–1515.
- 870 Lim, P. T., Sato, S., Van Thuoc, C., Tu, P. T., Huyen, N. T. M., Takata, Yoshida, M., Kobiyama,
871 A., Koike, K., Ogata, T., 2007. Toxic *Alexandrium minutum* (Dinophyceae) from
872 Vietnam with new gonyautoxin analogue. *Harmful Algae* 6(3), 321–331.

- 873 Lim, P. T., Usup, G., Leaw, C. P., Ogata, T., 2005. First report of *Alexandrium taylori* and
874 *Alexandrium peruvianum* (Dinophyceae) in Malaysia waters. Harmful Algae 4(2), 391–
875 400.
- 876 Lim, P.T., Yñiguez, A., Leaw, C.P., 2020. The toxic marine thecate dinoflagellate *Pyrodinium*
877 *bahamense*. In: Shubba Rao, D.V. (Ed.), Dinoflagellates: Classification, Evolution,
878 Physiology and Ecological Significance. Nova Science Publisher, pp. 481–498.
- 879 Loeblich III, A., 1975. A seawater medium for dinoflagellates and the nutrition of *Cachonina*
880 *niei*. J. Phycol. 11(1), 80–86.
- 881 Long, M., Krock, B., Castrec, J., Tillmann, U., 2021. Unknown extracellular and bioactive
882 metabolites of the genus *Alexandrium*: A review of overlooked toxins. Toxins 13, 905.
- 883 Lundholm, N., Churro, C., Escalera, L., Fraga, S., Hoppenrath, M., Iwataki, M., Larsen, J.,
884 Mertens, K., Moestrup, Ø., Zingone, A. (2023). IOC-UNESCO Taxonomic Reference
885 List of Harmful Micro Algae. *Alexandrium* Halim, 1960. Available online at
886 <https://www.marinespecies.org/hab/aphia.php?p=taxdetails&id=109470>. Accessed on
887 2023-06-06.
- 888 MacKenzie, L., de Salas, M., Adamson, J., Beuzenberg, V., 2004. The dinoflagellate genus
889 *Alexandrium* (Halim) in New Zealand coastal waters: comparative morphology, toxicity
890 and molecular genetics. Harmful Algae 3(1), 71–92.
- 891 Ronquist, F., Teslenko, M., van der Mark, P., Ayres, D.L., Darling, A., Höhna, S., Larget, B.,
892 Liu, L., Suchard, M.A., Huelsenbeck, J.P., 2012. MRBAYES 3.2: Efficient Bayesian
893 phylogenetic inference and model selection across a large model space. Syst. Biol. 61,
894 539–542.
- 895 Schliep, K. P., 2011. phangorn: phylogenetic analysis in R. Bioinformatics 27(4), 592–593.

- 896 Scholin, C. A., Herzog, M., Sogin, M., Anderson, D. M., 1994. Identification of group and
897 strain-specific genetic markers for globally distributed *Alexandrium* (Dinophyceae). II.
898 Sequence analysis of a fragment of the LSU rRNA gene. *J. Phycol.* 30, 999–1011.
- 899 Seibel, P. N., Müller, T., Dandekar, T., Wolf, M., 2008. Synchronous visual analysis and editing
900 of RNA sequence and secondary structure alignments using 4SALE. *BMC Research*
901 *Notes*, 1(1), 1–7.
- 902 Swofford, D. L., 2001. PAUP* Phylogenetic Analysis Using Parsimony (*and Other Methods)
903 Version 4.04beta. Sinauer Associates, Sunderland, Massachusetts.
- 904 Teng, S. T., Lim, H. C., Lim, P. T., Dao, V. H., Bates, S. S., Leaw, C. P., 2014. *Pseudo-nitzschia*
905 *kodamae* sp. nov. (Bacillariophyceae), a toxigenic species from the Strait of Malacca,
906 Malaysia. *Harmful Algae* 34, 17–28.
- 907 Teng, S. T., Lim, H. C., Lim, P. T., Rivera-Vilarelle, M., Quijano-Scheggia, S., Takata, Y.,
908 Quilliam, M. A., Wolf, M., Bates, S. S., Leaw, C. P., 2015. A non-toxigenic but
909 morphologically and phylogenetically distinct new species of *Pseudo-nitzschia*, *P. sabit*
910 sp. nov. (Bacillariophyceae). *J. Phycol.* 51(4), 706–725.
- 911 Teng, S. T., Tan, S. N., Lim, H. C., Dao, V. H., Bates, S. S., Leaw, C. P., 2016. High diversity of
912 *Pseudo-nitzschia* along the northern coast of Sarawak (Malaysian Borneo), with
913 descriptions of *P. bipertita* sp. nov. and *P. limii* sp. nov. (Bacillariophyceae). *J.*
914 *Phycol.* 52(6), 973–989.
- 915 Terao, K., Ito, E., Murakami, M., Yamaguchi, K., 1989. Histopathological studies on
916 experimental marine toxin poisoning - III. Morphological changes in the liver and thymus
917 of male ICR mice induced by Goniiodomin A, isolated from the dinoflagellate
918 *Goniodoma Pseudogoniaulax*. *Toxicon* 27, 269–271.

- 919 Tillmann, U., John, U., 2002. Toxic effects of *Alexandrium* spp. on heterotrophic dinoflagellates:
920 an allelochemical defence mechanism independent of PSP toxins. Mar. Ecol. Prog. Ser.
921 230, 47–58.
- 922 Tillmann, U., Krock, B., Wietkamp, S., Beran, A., 2020. A Mediterranean *Alexandrium taylorii*
923 (Dinophyceae) strain produces Goniodomin A and lytic compounds but not paralytic
924 shellfish toxins. Toxins 12(9), 564.
- 925 Tillmann, U., Bantle, A., Krock, B., Elbrächter, M., Gottschling, M., 2021. Recommendations
926 for epitypification of dinophytes exemplified by *Lingulodinium polyedra* and molecular
927 phylogenetics of the Gonyaulacales based on curated rRNA sequence data. Harmful
928 Algae 104, 101956. <https://doi.org/10.1016/j.hal.2020.101956>
- 929 [Trainer, V.L., 2020. GlobalHAB. Evaluating, Reducing and Mitigating the Cost of Harmful](#)
930 [Algal Blooms: A Compendium of Case Studies. PICES Sci. Rep., No. 59, 107 pp.](#)
- 931 [Trainer, V.L., Yoshida, M., 2014. Proceedings of the workshop on economic impacts of harmful](#)
932 [algal blooms on fisheries and aquaculture. PICES Sci. Rep., No. 47, 85pp.](#)
- 933 Triki, H. Z., Laabir, M., Moeller, P., Chomérat, N., Daly-Yahia, O. K., 2016. First report of
934 goniodomin A production by the dinoflagellate *Alexandrium pseudogonyaulax*
935 developing in southern Mediterranean (Bizerte Lagoon, Tunisia). Toxicon 111, 91–99.
- 936 Usup, G., Leaw, C. P., Ahmad, A., Lim, P. T., 2002. Phylogenetic relationship of *Alexandrium*
937 *tamiyavanichii* (Dinophyceae) to other *Alexandrium* species based on ribosomal RNA
938 gene sequences. Harmful Algae 1, 59–68.
- 939 Wolf, M., Ruderisch, B., Dandekar, T., Schultz, J., Müller, T., 2008. ProfDistS:(profile-)
940 distance based phylogeny on sequence-structure alignments. Bioinformatics 24(20),
941 2401–2402.

- 942 Yñiguez A.T., Lim, P.T., Leaw, C.P., Jipanin, S.J., Iwataki, M., Benico, G., Azanza, R.V., 2021.
943 Over 30 years of HABs in the Philippines and Malaysia: What have we learned? Harmful
944 Algae. 102, 101776. doi: 10.1016/j.hal.2020.101776
- 945 Yuki, K., Fukuyo, Y., 1992. *Alexandrium satoanum* sp. nov. (Dinophyceae) from Matoya Bay,
946 Central Japan. J. Phycol. 28(3), 395–399.

947 **Figure legends**

948 **Fig. 1** *Alexandrium limii* sp. nov. (Strain DBS08). LM. (A–F) Live cells. (A–B) General size and
949 shape from ventral-dorsal views. *N*, nucleus. Note the rounded structure (arrow in A),
950 presumably a pyrenoid. (C) Newly divided pair of cells. (D–E) Different epifluorescence
951 illumination of the same cell showing chloroplast distribution (D) and the shape and position of
952 the SYTOX-Green stained nucleus (E) under blue light excitation. (F–J) Thecae of Solophenyl
953 Flavine-stained cells. (F) Cell outline. (G) Cell in ventral and (H) dorsal view. (I–J) Details of
954 sulcal plates. Sulcal plate labels: Sa, anterior sulcal; Ssa, left anterior sulcal; Ssp, left posterior
955 sulcal; Sda, right anterior sulcal; Sdp, right posterior sulcal; Sma, anterior median sulcal; Smp,
956 posterior median sulcal. Sp, posterior sulcal; Saca, anterior accessory; Sacp, posterior accessory.
957 Scales, 10 μm .

958
959 **Fig. 2** *Alexandrium limii* sp. nov. (Strain Atay99Shio-02). LM. Live cells. General size and
960 shape from ventral-dorsal (A–E, G, H), and ventral-apical (F) views. *N*, nucleus. (D, E) Newly
961 divided pair of cells. Note the ventral pore (arrow in F) and a central rounded structure (arrows in
962 E and H), presumably a pyrenoid. Scales, 10 μm .

963
964 **Fig. 3** *Alexandrium limii* sp. nov. (Strain Atay99Shio-02). LM. Thecae of Solophenyl Flavine-
965 stained cells under epifluorescence illumination. (A–C) Cells in ventral or ventral-apical, (D)
966 dorsal, (E) apical, and (F–G) antapical views. Note the line or groove on plate Sp (arrow in F).
967 (H–I) Details of sulcal plates. Sulcal plate labels: Sa, anterior sulcal; Ssa, left anterior sulcal; Ssp,
968 left posterior sulcal; Sda, right anterior sulcal; Sdp, right posterior sulcal; Sma, anterior median

969 sulcal; Smp, posterior median sulcal. Sp, posterior sulcal. (J) Detailed view of the ventral part
970 showing plates 1', 6'', and Sa. Scales, 10 μ m (A–G), 5 μ m (H–J).

971

972 **Fig. 4** *Alexandrium limii* sp. nov. (Strain DBS08). SEM. (A) Cell in ventral view. Note the
973 longitudinal (white arrow) and transverse (white arrowhead) flagella. (B–D) Cells in apical view
974 showing epithelial plates. (E) Detailed view of sulcal plates. Sulcal plate labels: Sa, anterior
975 sulcal; Ssa, left anterior sulcal; Ssp, left posterior sulcal; Sda, right anterior sulcal; Sdp, right
976 posterior sulcal; Sma, anterior median sulcal. Cells in (F) right-lateral view (F) and antapical
977 view (G). Scales, 10 μ m.

978

979 **Fig. 5** Diagrammatic representation of thecal plate arrangement of *Alexandrium limii* sp. nov.
980 (A) Ventral view. (B) Dorsal view. (C) Epithelial plates in apical view. (D) Hypothecal plates in
981 antapical view. Scales, 10 μ m.

982

983 **Fig. 6** *Alexandrium ogatae* sp. nov. (Strain LASpbB10). LM. (A–C) Live cells. (A) Subspherical
984 cell. (B–C) Newly divided pair of cells. (D–E) Different epifluorescence illumination shows the
985 shape and position of the SYTOX-Green stained nucleus, *N* (D), and chloroplast distribution
986 under blue light excitation (E). (F–N) Thecae of Solophenyl Flavine-stained cells under
987 epifluorescence illumination. (F) Apical view. (G–H) Antapical view. (I–J) Ventral view (I) and
988 dorsal view (J) of the same cell. (K) Ventral view showing details of sulcal plates. (L–M) Ventral
989 view (L) and dorsal view (M) of the same cell. (N) Details of sulcal plates. Note the presence of
990 pore on the anterior sulcal plate (Sa) (white arrows). Sulcal plate labels: Sa, anterior sulcal; Ssa,
991 left anterior sulcal; Ssp, left posterior sulcal; Sda, right anterior sulcal; Sdp, right posterior sulcal;

992 Sma, anterior median sulcal; Smp, posterior median sulcal; Saca, anterior accessory; Sacp,
993 posterior accessory. Scales, 10 μm .

994

995 **Fig. 7** *Alexandrium ogatae* sp. nov. (Strain LASpbB10). SEM. (A–C) Cells in ventral view. Note
996 the pore on the anterior sulcal plate (Sa) (white arrowhead) (A, C) and the sulcal lists (white
997 arrows) (B, C). (C) Cells in a two-cell chain. (D) Cell in dorsal view. (E–F) Cells in apical view.
998 Note the presence of an anterior attachment pore (aap) at the left margin of Po. (G) Cell in
999 antapical view. (H) Close-up of the posterior sulcal plate (Sp) showing the posterior attachment
1000 pore (pap). Scales, 10 μm (A–G), 2 μm (H).

1001

1002 **Fig. 8** Diagrammatic representation of thecal plate arrangement of *Alexandrium ogatae* sp. nov.
1003 (A) Ventral view. (B) Dorsal view. (C) Epithecal plates in apical view. (D) Hypothecal plates in
1004 antapical view. Scales, 10 μm .

1005

1006 **Fig. 9** *Alexandrium pseudogonyaulax* (Stain LATAG8). (A–H) LM. (A–C) Subspherical
1007 vegetative cells. *N*, nucleus. (D) Different epifluorescence illumination shows the shape and
1008 position of the SYTOX-Green stained nucleus, *N*, and (E) chloroplast distribution under blue
1009 light excitation. (F–H) Thecae of Solophenyl Flavine-stained cells under epifluorescence
1010 illumination. (F–G) Apical ventral view. Note the position of the ventral pore (Vp). (H) Detailed
1011 view of sulcal plates. Sulcal plate labels: Sa, anterior sulcal; Ssa, left anterior sulcal; Ssp, left
1012 posterior sulcal; Sda, right anterior sulcal; Sdp, right posterior sulcal; Sma, anterior median
1013 sulcal; Smp, posterior median sulcal; Saca, anterior accessory; Sacp, posterior accessory. (I–K)

1014 SEM. (I) Ventral view. The white arrow shows the longitudinal flagellum. (J) Apical view. (K)
1015 Antapical view. Scales, 10 μm .

1016
1017 **Fig. 10** *Alexandrium taylorii* (strain AY1T). LM. (A–G) Live cells. (A–E) General size and
1018 shape from ventral-dorsal view. (E) Newly divided pair of cells. (F, G) Two focal planes of the
1019 same cell in ventral-apical view. *N*, nucleus. Note the central rounded structure (arrows in A and
1020 F), presumably a pyrenoid. (H–O) Thecae of Solophenyl Flavine-stained cells under
1021 epifluorescence illumination. (H–L) Cells in ventral or ventral-apical view. (M, N) Detailed view
1022 of ventral epithelial plates. (O) Details of sulcal plates. Note the line or groove on plate Sp
1023 (arrowhead in O). Sulcal plate labels: Sa, anterior sulcal; Ssa, left anterior sulcal; Ssp, left
1024 posterior sulcal; Sda, right anterior sulcal; Sdp, right posterior sulcal; Sma, anterior median
1025 sulcal; Smp, posterior median sulcal; Sp, posterior sulcal. Scales, 10 μm (A–L, O) or 5 μm (M,
1026 N).

1027
1028 **Fig. 11** (A) Box plots showing morphometric comparisons among strains of *Alexandrium limii*
1029 (DBS08, DBS28, Atay99Shio-02), *A. ogatae* (LASpbB10, LASpbD3), *A. pseudogonyaulax*
1030 (LaTAG8, LMIAE9), and *A. taylorii* (AY1T, AY7T). (B) Principal component analysis (PCA)
1031 ordination showing the multivariate variation among the strains with respect to the morphometric
1032 measurements, ellipses represent 95% confidence intervals for different strains (filled) and
1033 species (line). Vector directions indicate the morphometric traits' contribution to the first two
1034 dimensions.

1035

1036 **Fig. 12** Phylogenetic trees based on the SSU, LSU rDNA, ITS1-5.8S-ITS2, and ITS2 sequence-
1037 structure datasets of *Alexandrium* species. Nodal supports are bootstrap values of maximum
1038 parsimony (MP), maximum likelihood (ML), and Bayesian inference (BI), with only >50%
1039 supports shown. Nodal supports of 100% for all three analyses are marked with thick lines. See
1040 Supplementary Figs S1–S3 for detailed phylogenetic inferences.

1041
1042 **Fig. 13** ITS2 RNA transcripts of *A. limii* sp. nov. (A) and *A. ogatae* sp. nov. (B). The rectangles
1043 indicate the positions of compensatory base changes (CBCs) or hemi-CBCs (HCBCs) when
1044 compared to other closely related species, were observed. (C) Pairwise comparison of the
1045 number of CBCs (lower diagonal) and HCBCs (upper diagonal) among the closely related
1046 species.

1047
1048 **Fig. 14** A dichotomous diagram of diagnostic thecal features of *Alexandrium* species with
1049 metasert/exsert first apical plate (1'). Note that there is a Genbank LSU sequence AF032348.1
1050 annotated as *A. concavum*, but this strain, based on morphology presented in MacKenzie et al.
1051 (2004), is *A. gaarderae* L.Nguyen-Ngoc & J.Larsen, a species with an elongated rhomboid
1052 1' contacting the pore plate.

1053 **Supplementary Figures**

1054 **Fig. S1** Phylogenetic tree based on SSU rDNA sequences of *Alexandrium* species. Nodal
1055 supports are bootstrap values of maximum parsimony (MP), maximum likelihood (ML), and
1056 Bayesian inference (BI), with only >50% supports shown.

1057

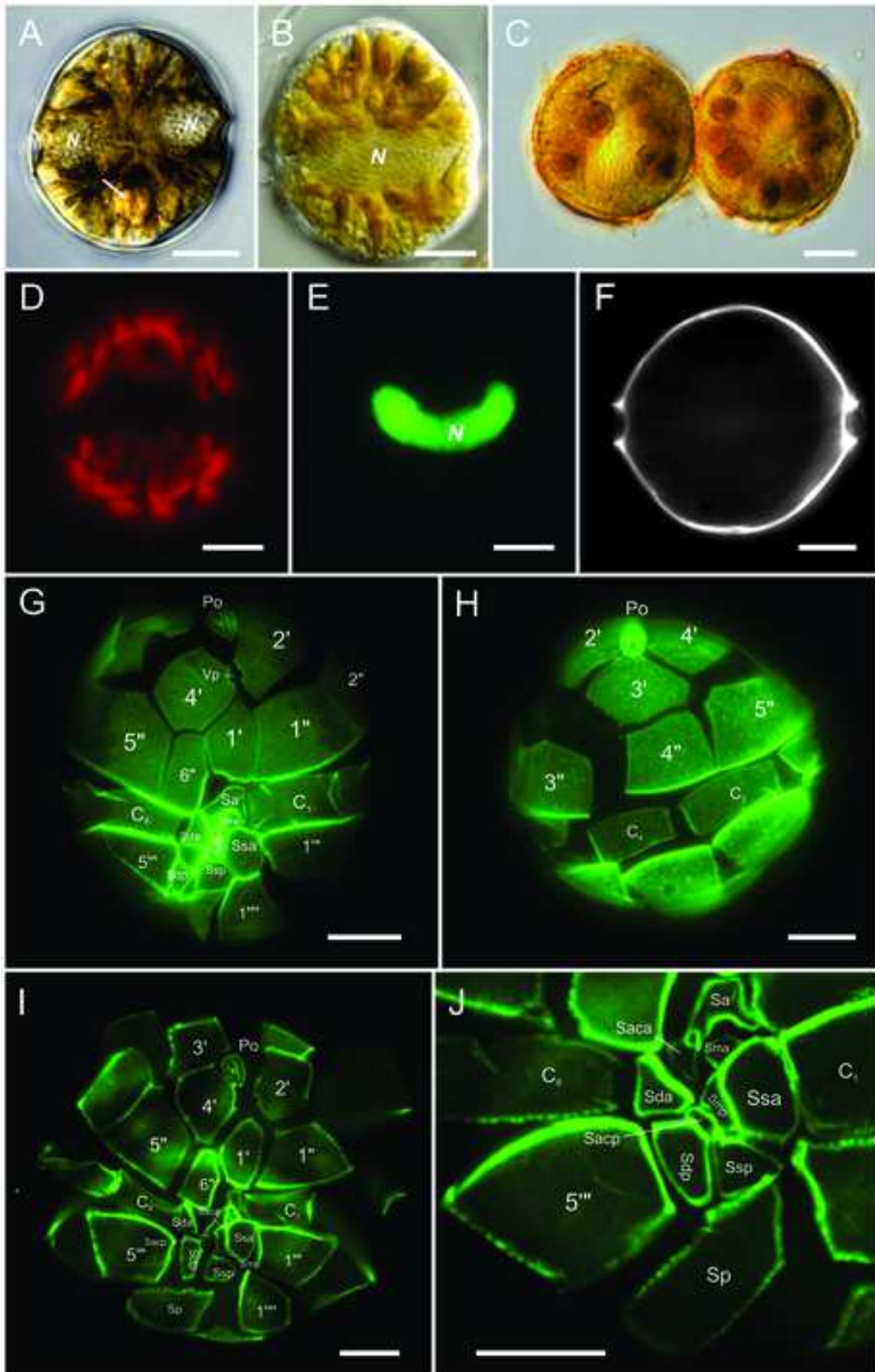
1058 **Fig. S2** Phylogenetic tree based on LSU rDNA sequences of *Alexandrium* species. Nodal
1059 supports are bootstrap values of maximum parsimony (MP), maximum likelihood (ML), and
1060 Bayesian inference (BI), with only >50% supports shown.

1061

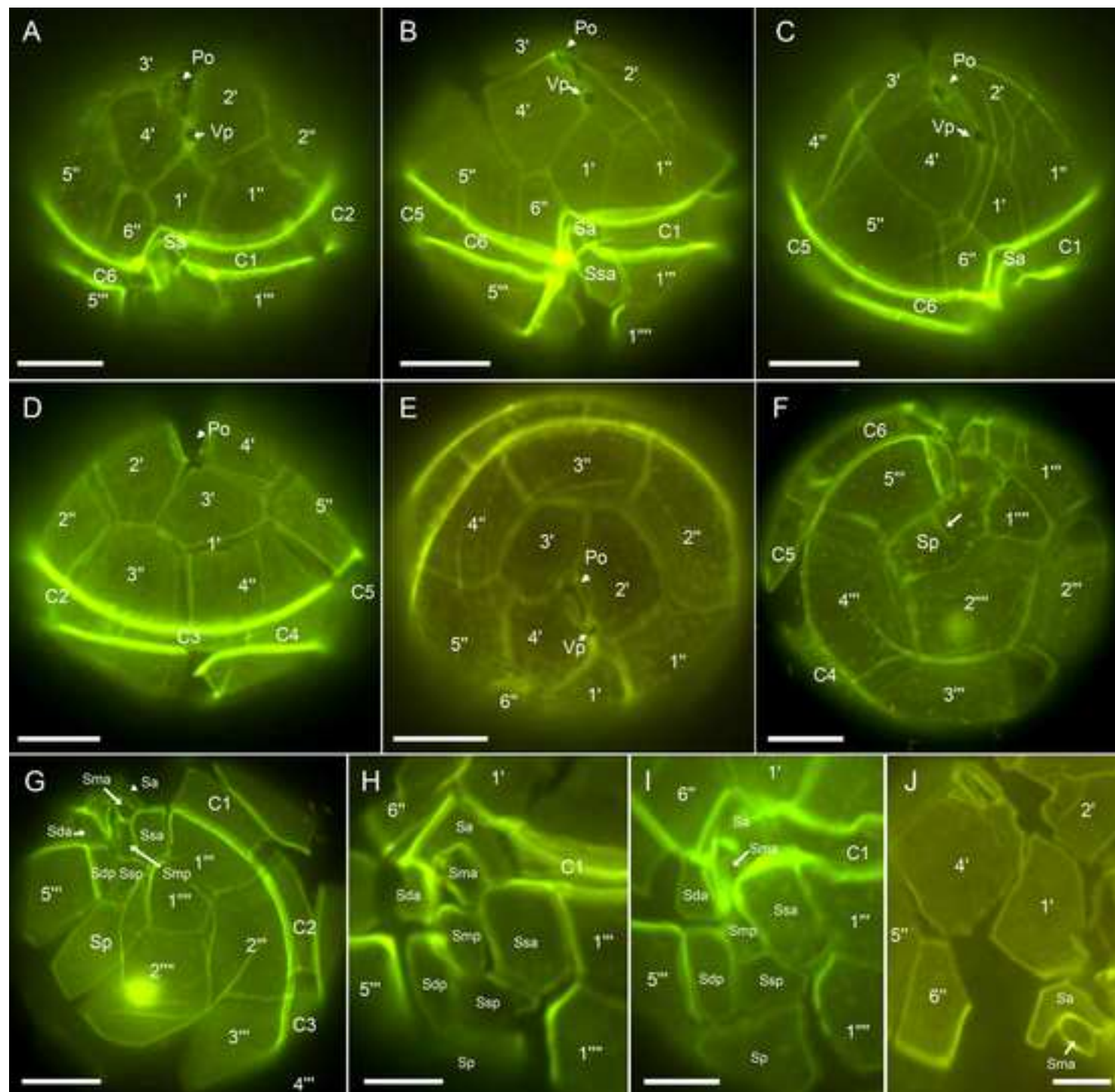
1062 **Fig. S3** Phylogenetic tree based on ITS rDNA sequences of *Alexandrium* species. Nodal supports
1063 are bootstrap values of maximum parsimony (MP), maximum likelihood (ML), and Bayesian
1064 inference (BI), with only >50% supports shown.

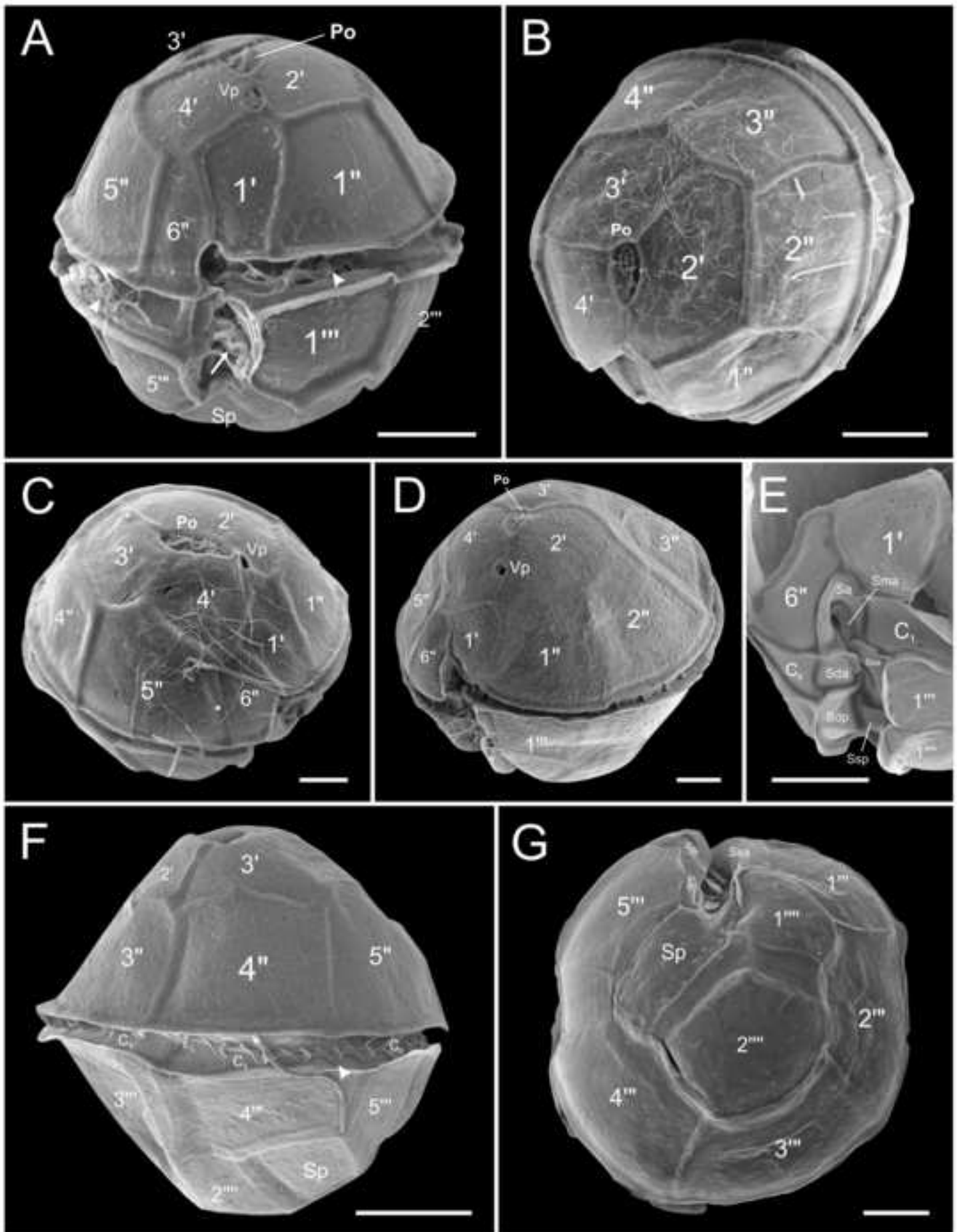
1065

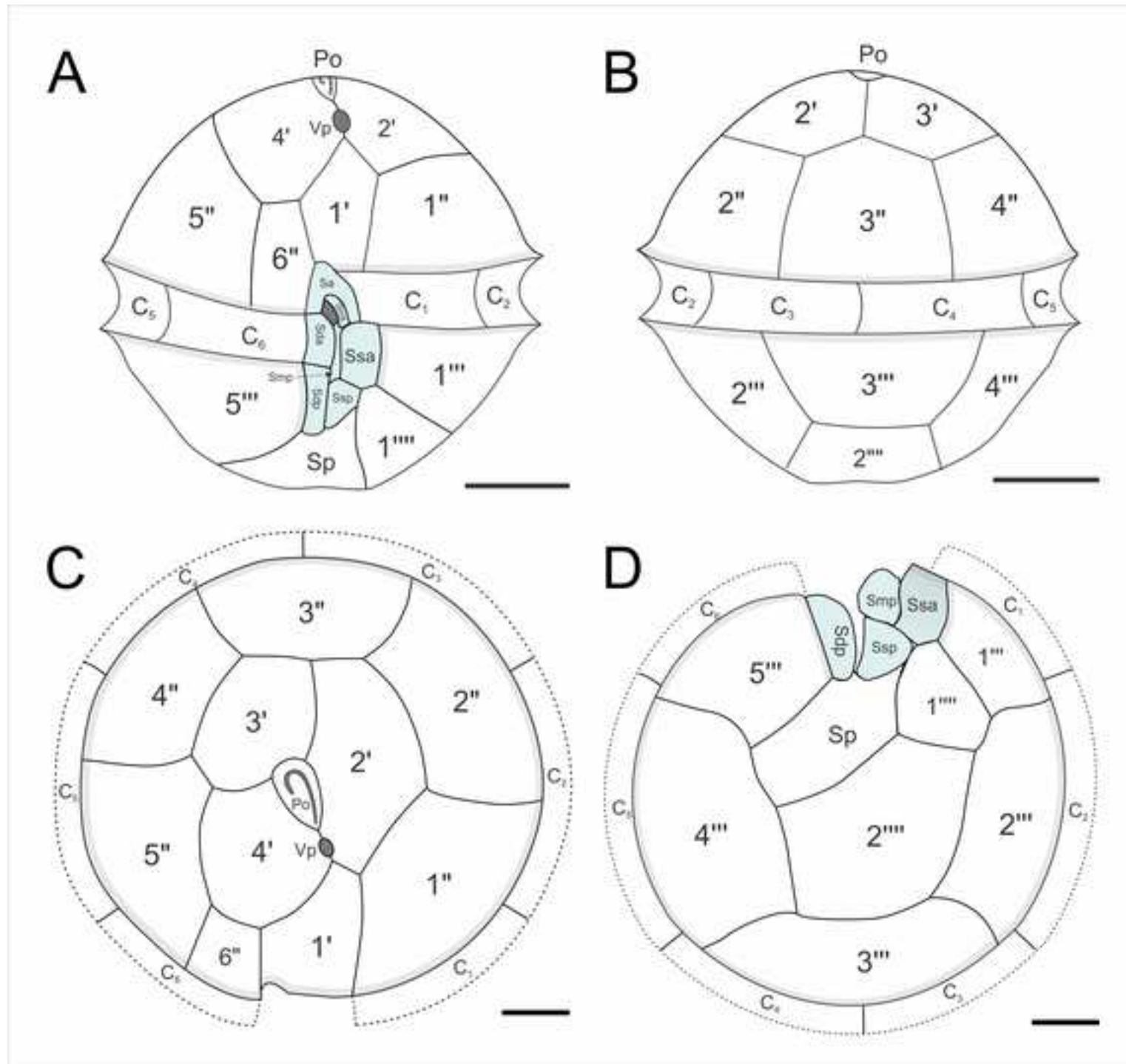
1066 **Supplementary Material 1:** Morphometric data of *Alexandrium limii*, *A. ogatae*, *A.*
1067 *pseudogonyaulax*, and *A. taylorii*. [xlsx file]

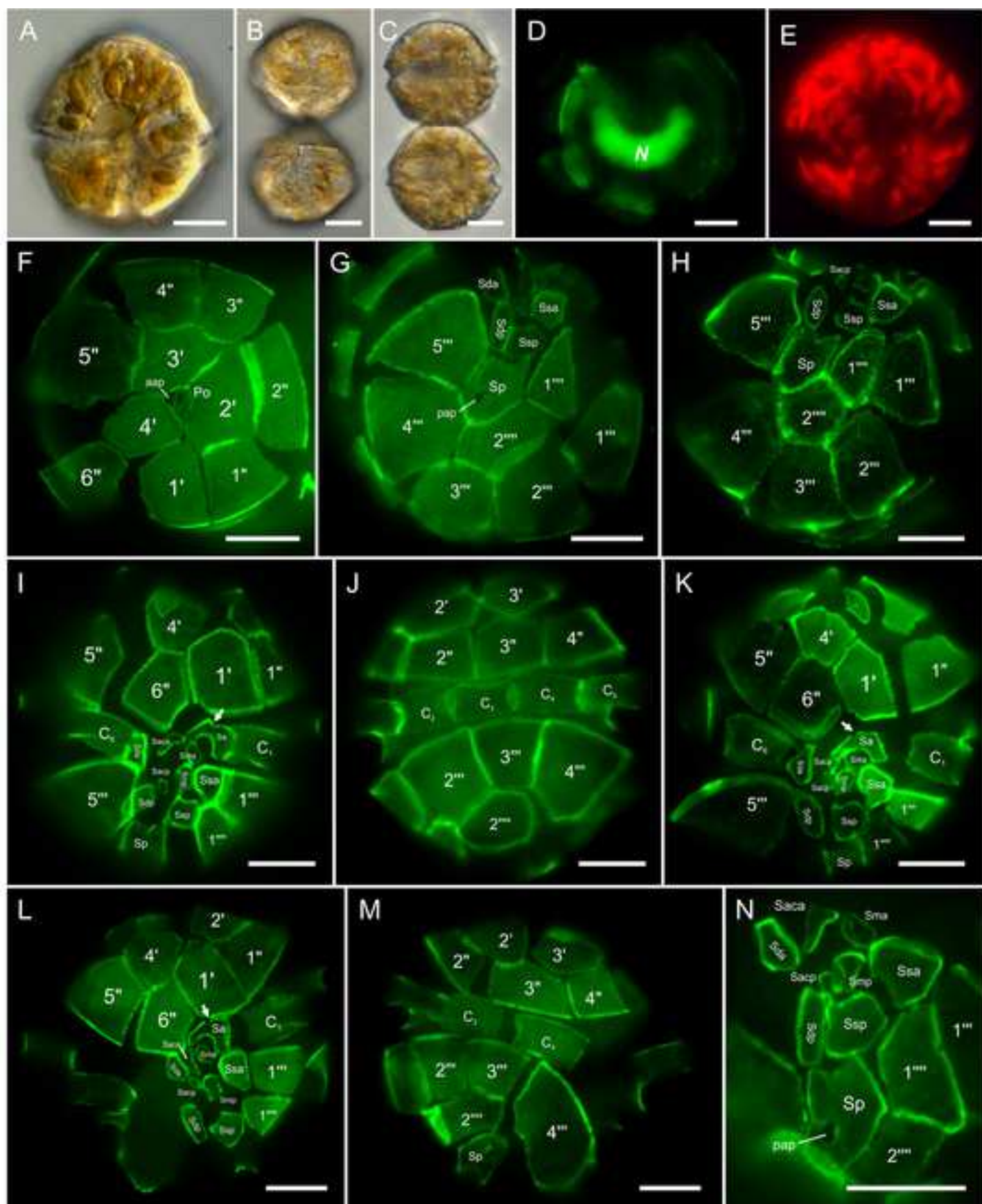


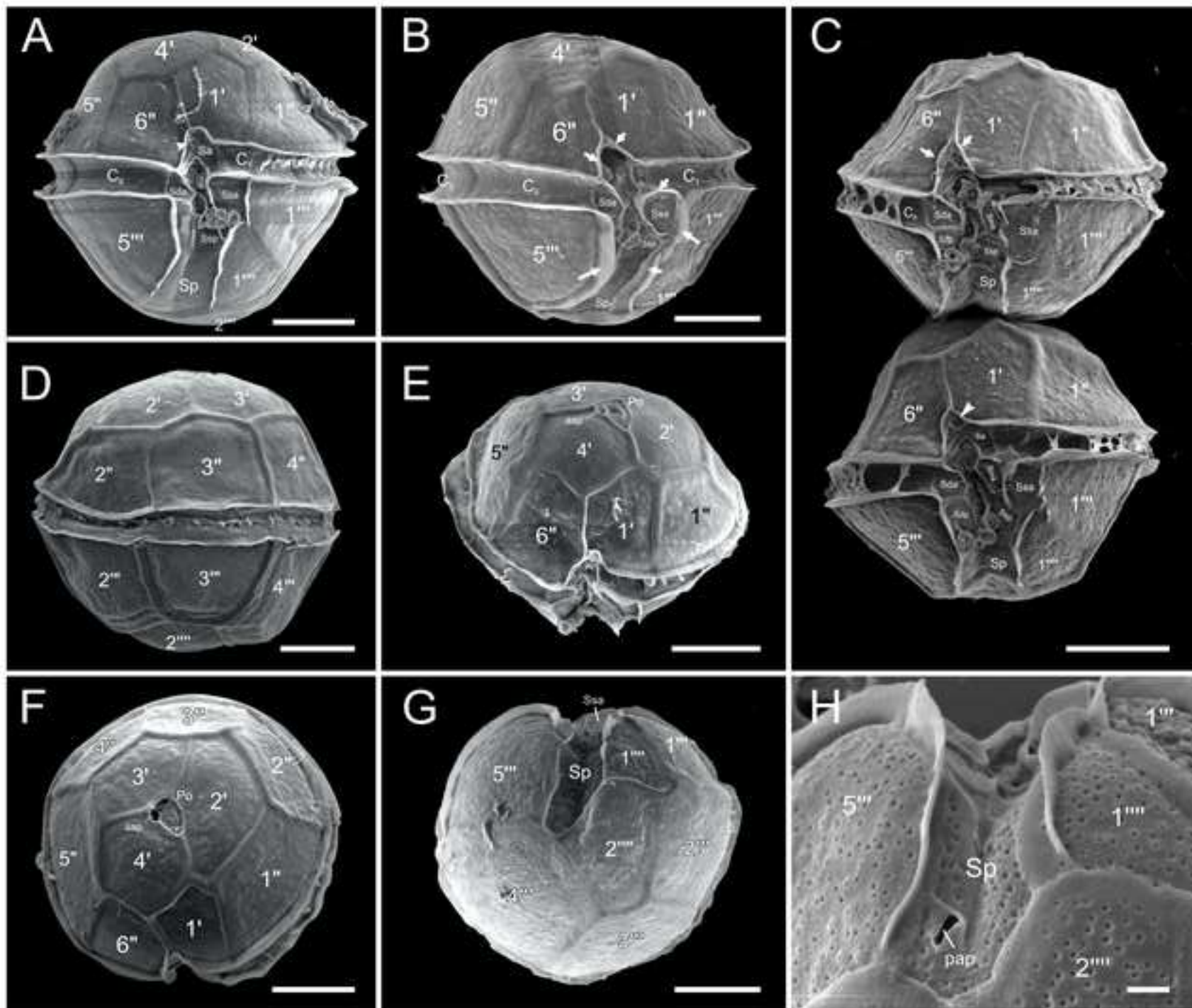


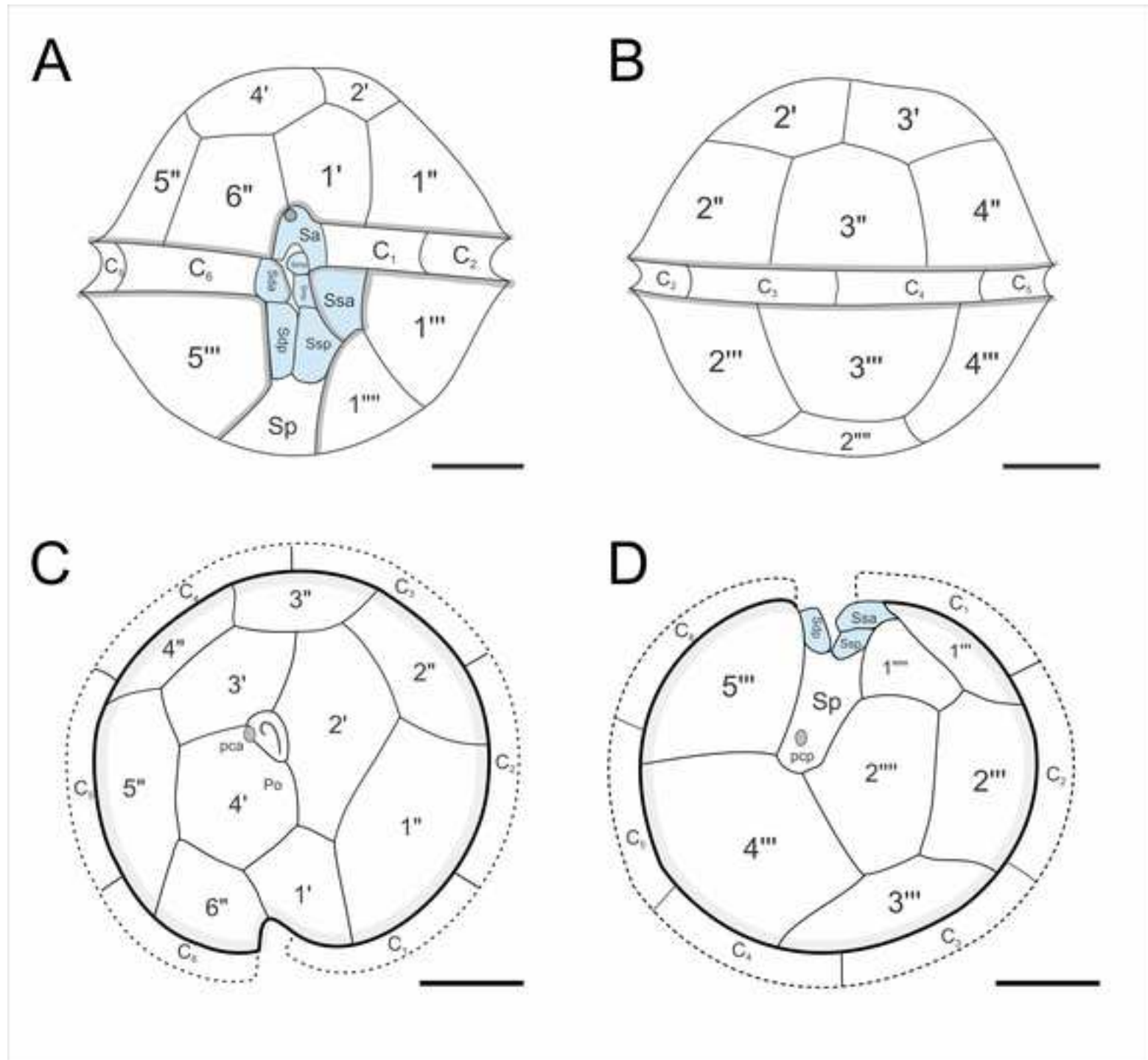


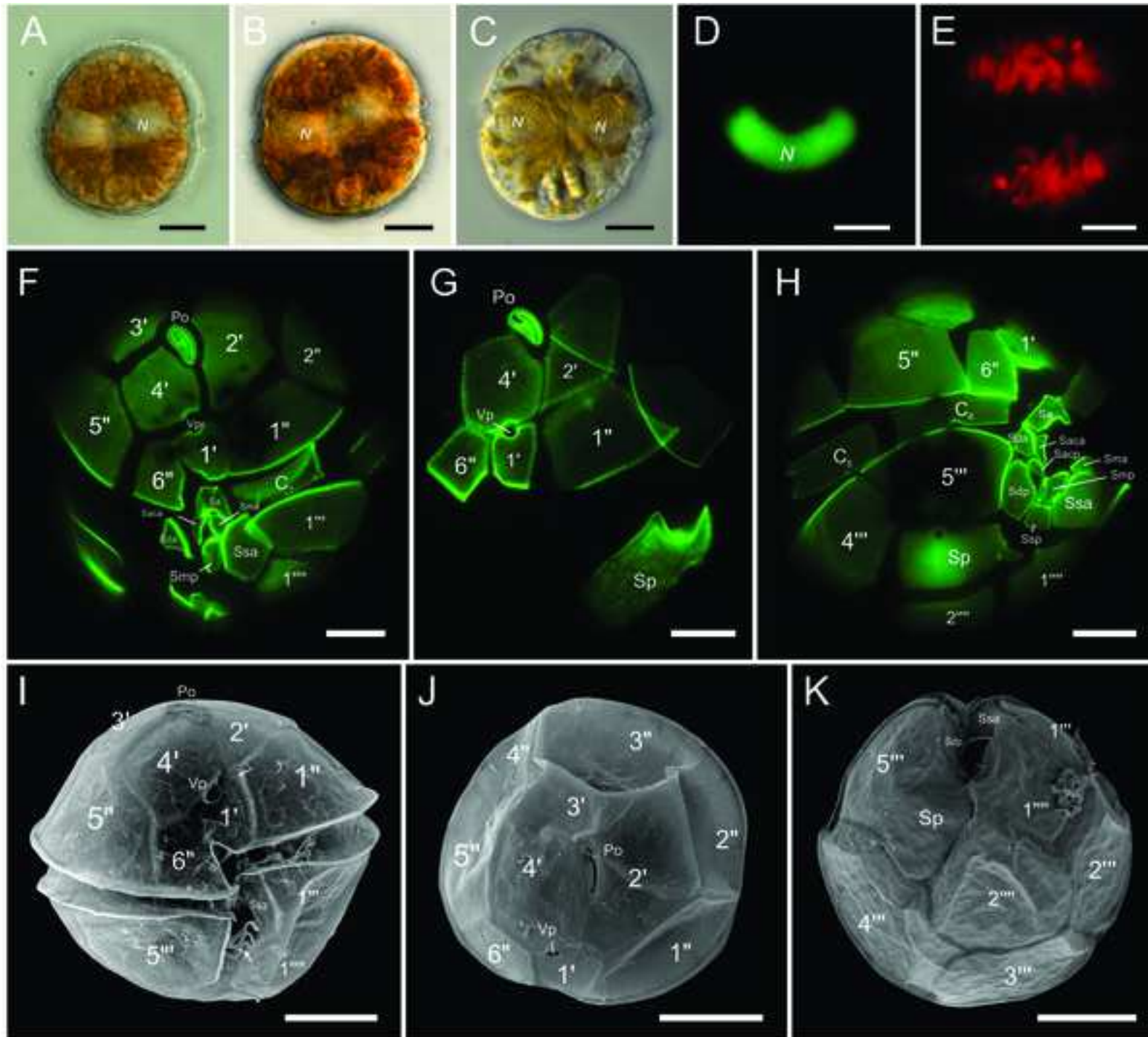


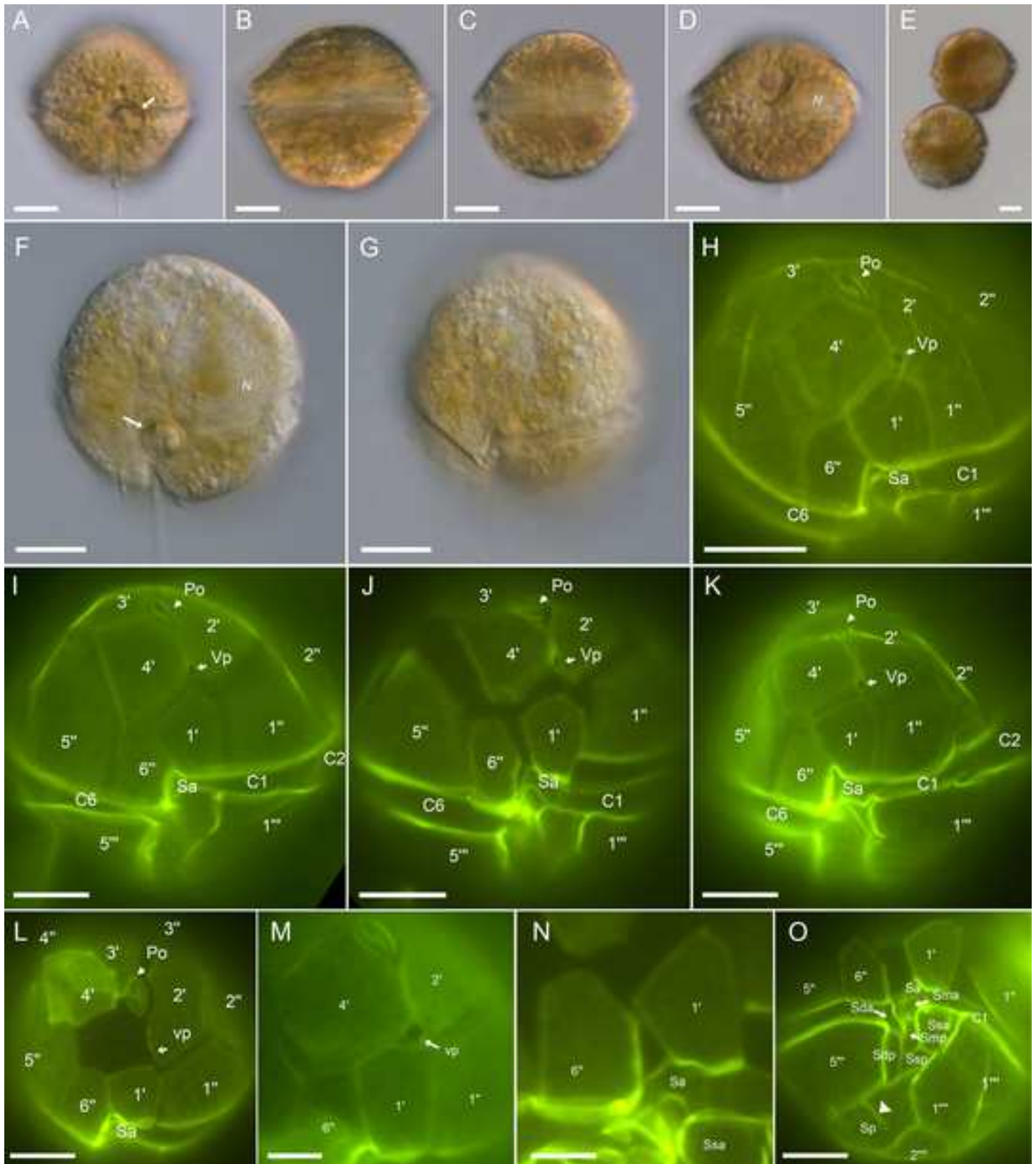


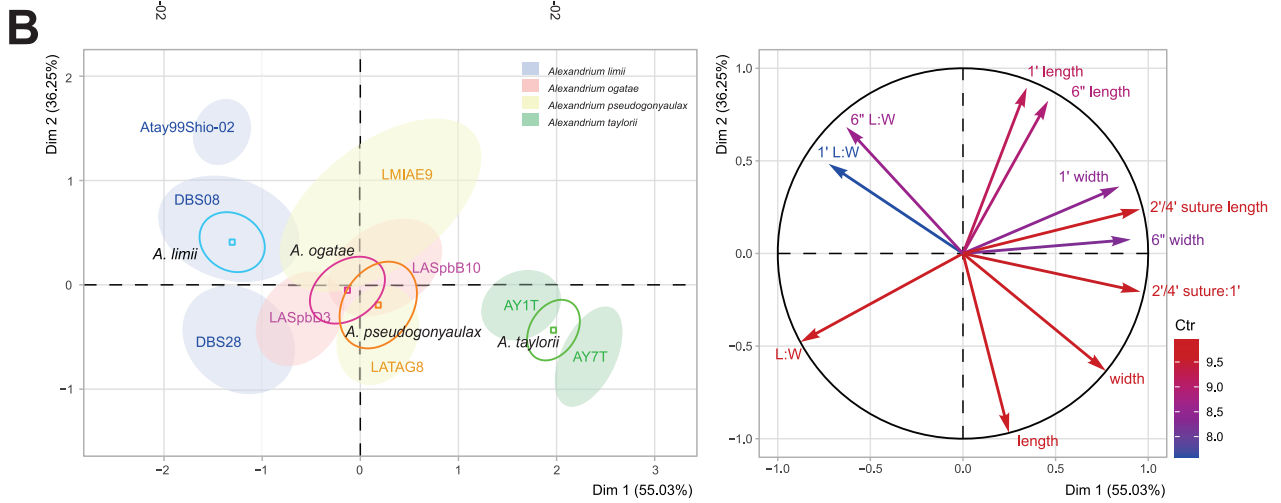
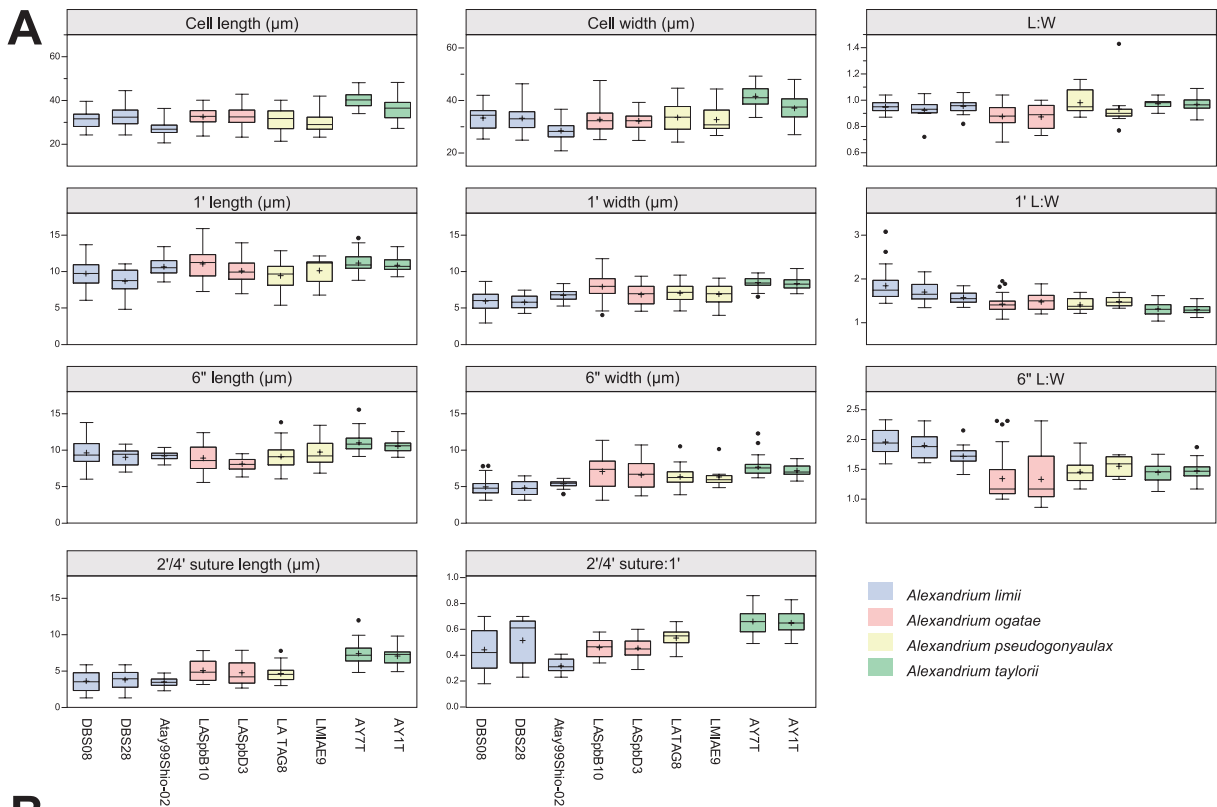


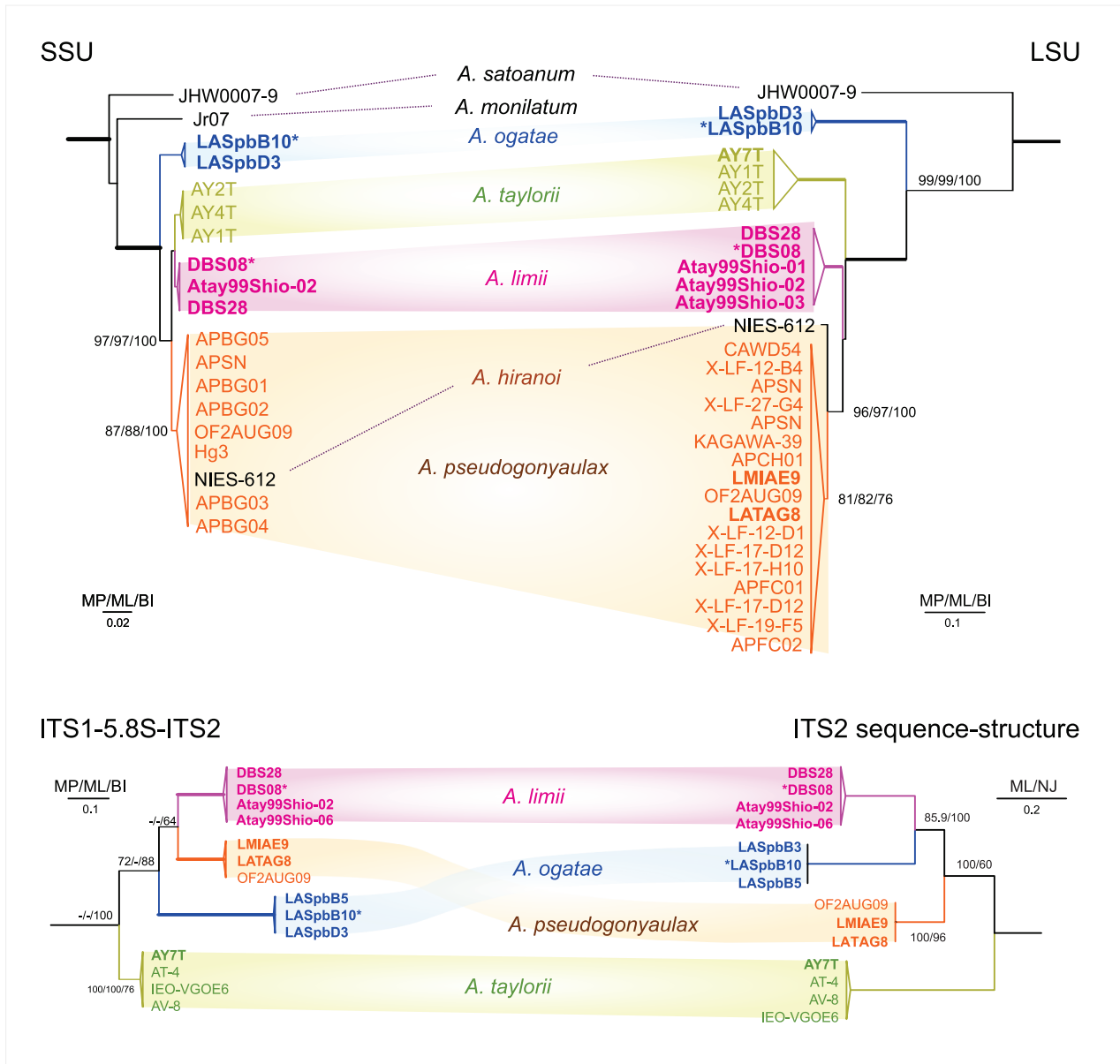


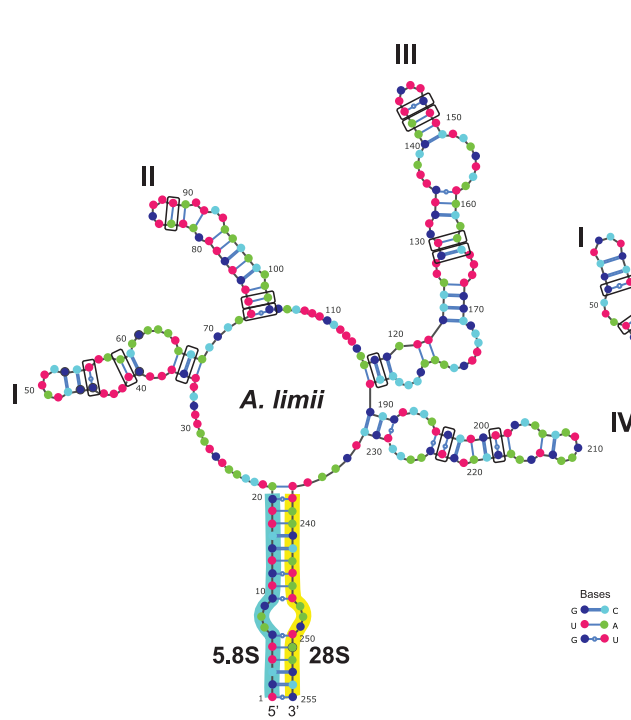
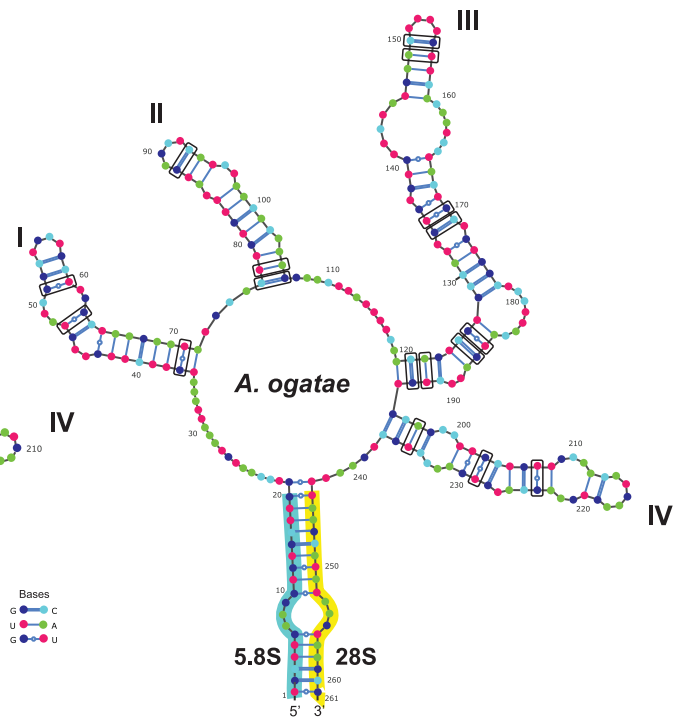










A. ITS2 transcript of *A. limii*

B. ITS2 transcript of *A. ogatae*

C. Pairwise comparison of CBCs (lower panel) and HCBCs (upper panel)

	<i>a</i>	<i>b</i>	<i>c</i>	<i>d</i>	
<i>A. pseudogonyaulax</i>	<i>a</i>	0	8	6	2
<i>A. ogatae</i>	<i>b</i>	2	0	6	5
<i>A. limii</i>	<i>c</i>	0	1	0	3
<i>A. taylorii</i>	<i>d</i>	0	0	0	0

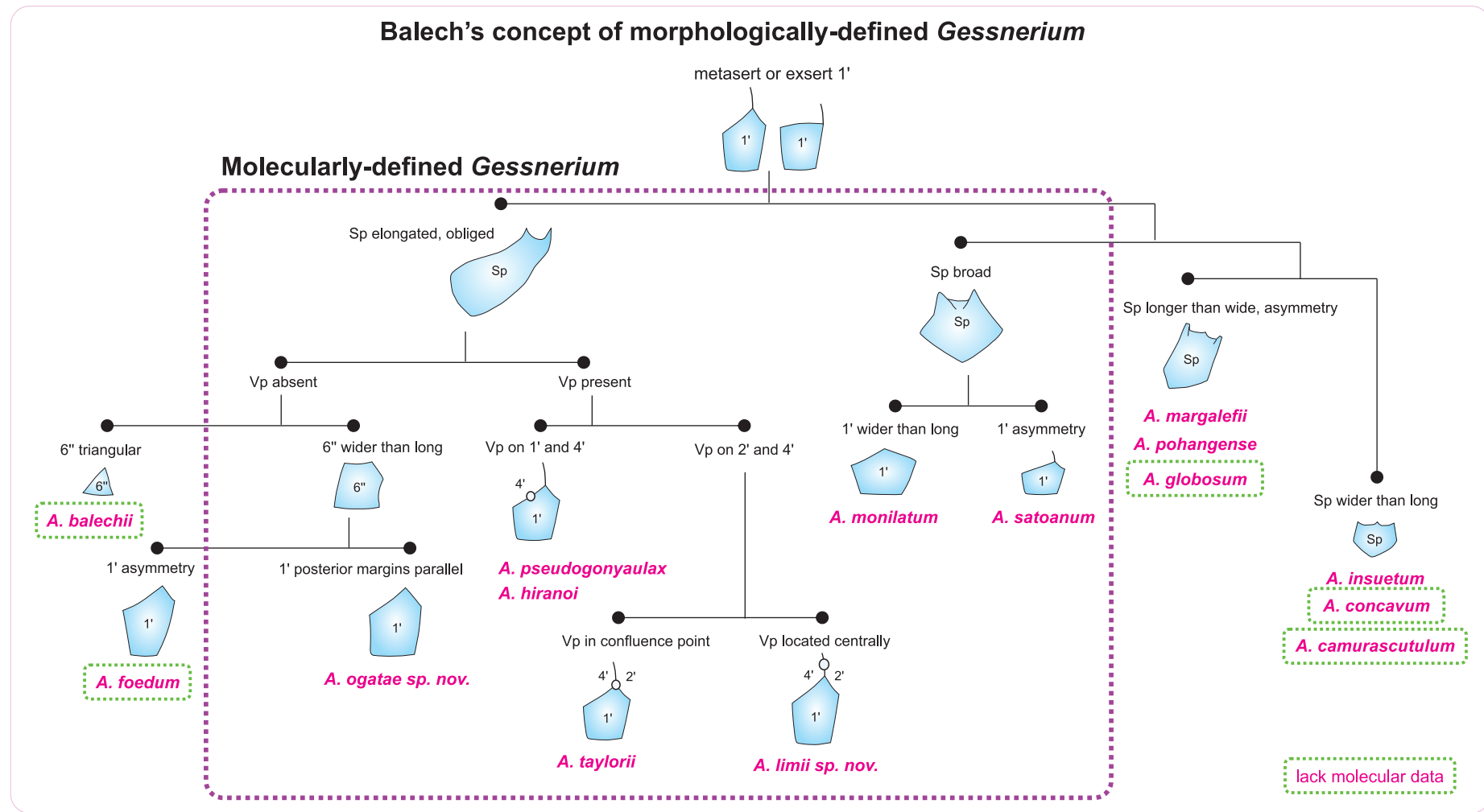


Table 1. Information of *Alexandrium* species and strains used in this study, including locations, date of collection, temperature and salinity of culture condition, morphological and toxicity information, GenBank accession numbers of the SSU, LSU, and ITS rDNA sequences, and references. *, type specimen. +, morphology/toxicity tested; –, morphology/toxicity not tested.

Species	Strain	Location	Date of collection	Temperature/salinity	Morphology/Toxicity	GenBank accession number			Reference
						SSU	LSU	ITS	
<i>A. limii</i>	DBS08 *	Batang Salak (Malaysia) 1° 36' 31.4886" N, 110° 19' 36.6774" E	Mar 2017	26°C/ 30	+/+	OP782553	OK271124	OK274344	This study
<i>A. limii</i>	DBS28	Batang Salak (Malaysia) 1° 36' 31.4886" N, 110° 19' 36.6774" E	Mar 2017	26°C/ 30	+/-	OP782554	OK271125	OK274343	This study
<i>A. limii</i>	Atay99Shio-02	Shioya Bay, Okinawa (Japan)	Jul 1999	20°C/ 32	+/+	LC770197	AB607264	LC770198	This study; Nagai & Itakura, 2012
	Atay99Shio-01	Shioya Bay, Okimawa (Japan)	Jul 1999	20°C/ 32	-/-	–	AB607263	–	This study; Nagai & Itakura, 2012
	Atay99Shio-03	Shioya Bay, Okinawa (Japan)	Jul 1999	20°C/ 32	-/-	–	AB607265	–	This study; Nagai & Itakura, 2012
	Atay99Shio-06	Shioya Bay, Okinawa (Japan)	Jul 1999	20°C/ 32	-/-	–	–	AB841262	This study; Nagai, 2013
<i>A. ogatae</i>	LASpbB10 *	Sepanggar Bay (Malaysia)	Sep 2018	26°C/ 30	+/+	OP782555	OK271127	OK274341	This study

Species	Strain	Location	Date of collection	Temperature/salinity	Morphology/Toxicity	GenBank accession number			Reference
						SSU	LSU	ITS	
<i>A. ogatae</i>	LASpbB5	6° 5' 29.3388" N, 116° 7' 39.2772" E Sepanggar Bay (Malaysia)	Aug 2018	26°C/ 30	-/-	-	OK271126	OK274342	This study
<i>A. ogatae</i>	LASpbD3	6° 5' 29.3388" N, 116° 7' 39.2772" E Sepanggar Bay (Malaysia)	Sep 2018	26°C/ 30	+/+	OP782556	OK271128	OK274340	This study
<i>A. pseudogonyaulax</i>	LMIAE9	6° 5' 29.3388" N, 116° 7' 39.2772" E Lumut (Malaysia)	Oct 2017	26°C/ 30	+/-	-	OK271130	OK274338	This study
<i>A. pseudogonyaulax</i>	LATAG8	4° 12' 35.2" N, 100° 36' 02.6" E Telaga Air (Malaysia)	Aug 2018	26°C/ 30	+/-	-	OK271129	OK274339	This study
<i>A. taylorii</i>	AY1T	1° 40' 35.6" N, 110° 12' 35.3" E Lagoon of Marano (Italy)		20°C/ 32	+/+	AJ535390	AJ535347	-	This study; Tillmann and John, 2002
<i>A. taylorii</i>	AY7T	Lagoon of Marano (Italy)		20°C/ 32	+/+	-	MT643180	MT644478	This study; Tillmann et al., 2020

Table 2. Toxins profiles and cell quotas of the investigated *Alexandrium* strains. For *A. limii* strain Atay99Shio-02, three different cell pellets obtained from three independently grown cultures have been analyzed for lipophilic toxins. nd, not detected. The number of cells analyzed for each species/strain/pellet and the limit of detection (LOD) for lipophilic toxins and for individual PST compounds are listed in Suppl. Tables S2–S3.

Species (strain)	lipophilic toxins			Hydrophilic toxins		
	Goniodomins [pg cell ⁻¹]			SPX	GYM	PSTs
	GDA	34-desM-GDA	9-desM-GDA			
<i>A. limii</i> (DBS08)	12.9	nd	nd	nd	nd	nd
<i>A. limii</i> (Atay99Shio-02)	nd	7.3	nd	nd	nd	nd
<i>A. limii</i> (Atay99Shio-02)	nd	1.4	nd	nd	nd	nd
<i>A. limii</i> (Atay99Shio-02)	nd	7.2	nd	nd	nd	nd
<i>A. ogatae</i> (LASpbB10)	13.7	nd	nd	nd	nd	nd
<i>A. ogatae</i> (LASpbD3)	6.3	nd	nd	nd	nd	nd
<i>A. taylorii</i> (AY1T)	6.8	nd	0.6	nd	nd	nd
<i>A. taylorii</i> (AY7T*)	11.7	nd	nd	nd	nd	nd

*data from Tillmann et al. (2020)



Click here to access/download

Supplementary Material

Suppl Mat 1. Alex morphometrics Summary
Statistics.xlsx



Click here to access/download
Supplementary Material
Fig. S1 SSU tree.pdf





Click here to access/download
Supplementary Material
Fig. S2 LSU tree.pdf





Click here to access/download
Supplementary Material
Fig. S3 ITS tree.pdf





Click here to access/download
Supplementary Material
Suppl Tables_v.8.docx



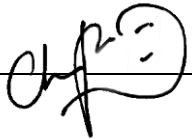
HARMFUL ALGAE AUTHOR DECLARATION

Submission of an article implies that the work described has not been published previously (except in the form of an abstract or as part of a published lecture or academic thesis), that it is not under consideration for publication elsewhere, that its publication is approved by all authors and tacitly or explicitly by the responsible authorities where the work was carried out, and that, if accepted, it will not be published elsewhere in the same form, in English or in any other language, without the written consent of the copyright-holder.

By attaching this Declaration to the submission, the corresponding author certifies that:

- The manuscript represents original and valid work and that neither this manuscript nor one with substantially similar content under the same authorship has been published or is being considered for publication elsewhere.
- Every author has agreed to allow the corresponding author to serve as the primary correspondent with the editorial office, and to review the edited typescript and proof.
- Each author has given final approval of the submitted manuscript and order of authors. Any subsequent change to authorship will be approved by all authors.
- Each author has participated sufficiently in the work to take public responsibility for all the content.

I am the corresponding author signing on behalf of all co-authors of the manuscript:

Name	Signature	Date signed
Chui Pin Leaw		25 Apr 2023

Declaration of interests

The authors declare that they have no known competing financial interests or personal relationships that could have appeared to influence the work reported in this paper.

The authors declare the following financial interests/personal relationships which may be considered as potential competing interests: